ChemPubSoc Europe

DOI: 10.1002/ejic.201700735

EurJIC European Journal of Inorganic Chemistry

Microreview

CLUSTER ISSUE

Gold Nanoprobes

Towards Ultra-Bright Gold Nanoclusters

Andrea Cantelli,[a] Gloria Guidetti,[a] Jeannette Manzi,[a] Valeria Caponetti,[a] and Marco Montalti*[a]

Abstract: Fluorescence bioimaging is a non-invasive technique that permits to investigate living organism in real time with high tridimensional resolution. Properly engineered fluorescent (or photoluminescent) nanoparticles promise to surpass conventional fluorescent molecular probes as contrast agent. Photoluminescent semiconductor quantum dots show, for example, enhanced brightness and photostability. Concerns arising from the toxic metal content of quantum dots prompted the search for alternative inorganic nanoparticles with similar properties but less hazardous. Gold is almost unanimously considered to be highly tolerated by living organism and the environment. Nevertheless, although photoluminescence of gold nanocluster is known by decades, brightness of these nanoparticles has typically reported to be low, mostly because of the poor photoluminescence quantum yield (< 1 %). Different approaches have been proposed to enhance this poor quantum yield aiming to achieve ultra-bright gold nanoparticles with features superior to conventional dyes. Here most relevant and recent results in this direction are summarized and critically discussed.

1. Introduction

Fluorescence, and more in general photoluminescence (PL), is a powerful tool for investigating living organisms in real time and space, both in vivo and in vitro.[1,2] As main advantage ompared to other diagnostic approaches, optical techniques exploit poorly invasive radiations both for probing and analyzing the biological samples. Intrinsic fluorescence of biological tissues is typically moderate and unspecific and it gives poor structural and functional information. The use of fluorescent probes (typically organic fluorophores)[3] as contrast agent, is hence fundamental in order to investigate the morphology of biological targets as well as the biochemical process occurring in specific biological compartments.

In the last decades, thanks to the advent of nanotechnology and nanochemistry, the use of ultra-bright nanoparticles (NPs), has been proposed as an innovative and advantageous alternative to molecular probes.[4] In particular, inorganic probes based on cadmium and lead containing inorganic quantum dots, if properly designed, are highly photostable and bright in physiological conditions.[5] Moreover, their emission wavelength is tunable and suitable for in-vivo applications. Recent concerns about the safety of these potentially toxic nanomaterials have prompted the research of alternative inorganic nanoprobes composed of safer elements.[6] Gold NPs have found widespread application in bioimaging[7] and nanomedicine[8] demonstrating high biocompatibility.[6b] Nevertheless, the first investigators who observed the PL of gold NPs reported PL QY of the order of 0.1 % or lower,[9] hence not suitable for fluorescence imaging.

Improving the poor PL brightness of Au NPs was a real challenge and involved a wide interdisciplinary scientific community including chemists, physicists, biologists and engineers. Thanks to their effort, highly bright gold NPs, or more precisely nanoclusters (NCs) with PL QY as high as 40–60 %, tunable visible to near infrared (NIR) emission, small hydrodynamic size and high biocompatibility have been produced. Finally, the applicability of gold NCs as PL probe for in vitro and in vivo imaging has been demonstrated.[10]

Although, achieving ultra-bright[11] Au NCs, with features that make them actually superior to conventional fluorescent probe, is still challenging. Most recent advances in this direction

[a] *Department of Chemistry "G. Ciamician", University of Bologna, Via Selmi 2, 40126 Bologna, Italy*
E-mail: marco.montalti2@unibo.it
https://www.unibo.it/sitoweb/marco.montalti2
ORCID(s) from the author(s) for this article is/are available on the WWW under https://doi.org/10.1002/ejic.201700735.

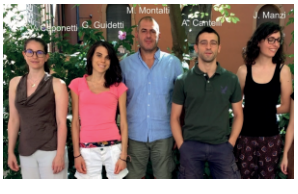

Marco Montalti received his PhD in Chemical Sciences in 2001 from the University of Bologna (UNIBO) where now he is associate professor. In 2002 he started his independent research career in the field of luminescent silica and metal nanoparticles for sensing, catalysis and bioimaging. The main research topic of his group is the design, production, and characterization of ultrabright, biocompatible and stimuli-responsive luminescent nanostructures for application to in vitro and in vivo bioimaging.
Andrea Cantelli is a post-doc fellow at UNIBO who earned his PhD in Chemical Science in 2016 working on a project aimed to develop ultra-bright Au NCs.
Gloria Guidetti, Jeannette Manzi and Valeria Caponetti are PhD students working on the development of nanostuctured photoresponsive systems for optical imaging and catalysis.

and most promising strategies conceived to enhance the PL brightness of Au NCs are summarized and discussed in this microreview.

1.1 What are Au NCs?

PL is peculiar of small gold NPs: roughly, only particles with a diameter below 2 nm show detectable light emission.[12] NPs of these sizes show discrete electronic states due to the strong quantum confinement effect[13] and present optical and electronic molecular-like properties. For these reasons they are specifically classified as Au NCs in order to distinguish them from larger Au NPs.[7,8,12a,14] Stabilization of Au NCs in solution typically exploits surface functionalization with suitable organic ligands.[14b,15] In order to achieve specific interaction and to produce protected nanoparticle high affinity of the ligand for the gold surface is required and organic thiolate are the first choice ligands.[16] The use of optimal thiolate ligands was a key strategy for the preparation of molecular like gold clusters with well-defined atomic composition.[14b] These atomically precise thiolate protected golds NCs can be described with the general formula $Au_n(SR)_m$, where R is a generic organic residual.

Some of the bright, PL Au NCs discussed in this microreview have not been clearly demonstrated to be atomically precise species, moreover NCs with stabilizing ligand other than thiolate will be considered. Nevertheless, particular consideration will be devoted to discuss the properties of Au-thiolate atomically precise NCs since they represent an essential model for understanding the correlation between the PL properties and the structure/composition features.

1.2 What is Brightness?

Brightness (B) allows to quantify the actual fluorescence or, more in general, photoluminescence (PL) signal generated by an emitter (e.g. a molecule or a NP) in given excitation conditions, and it is the product of its molar absorption coefficient (ε) and of the PL quantum yield (QY).[4b] In the low concentration regime, typical of imaging applications, hence, the PL intensity is directly proportional to $B = \varepsilon \times QY$.

Optimization of the PL QY is fundamental to achieve ultrabright PL probes but not less important is the efficiency of absorbing excitation light ε. A simple and powerful, but still largely unexplored, strategy to enhance brightness of Au NCs is the use of ligands able to harvest excitation light and transfer the excitation energy to the metal core, as schematized in Figure 1.

It is worth noting that, according to the definition, B is dependent on the excitation wavelength but not on the emission one. For application to bioimaging, indeed, both excitation and emission spectral signatures are important: probes with absorption/emission in the red/NIR region guarantee a minimal background due to intrinsic fluorescence of biomolecules (auto-fluorescence). NIR region is optimal for in vivo fluorescence imaging since biological tissues present the highest transparency in this spectral window.[2m,17]

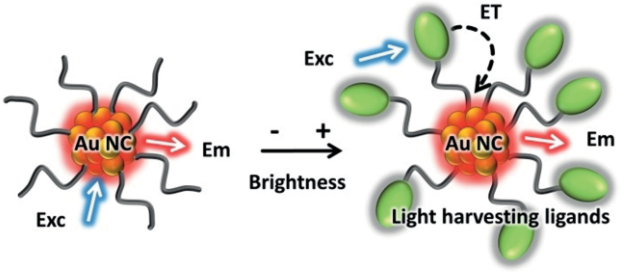

Figure 1. PL brightness of Au NCs (left) can be enhanced by introducing ligands able to absorb efficiently the excitation light and to sensitize via energy transfer (ET) the emission of the gold core (right).

2. Synthesis of Au NCs

A detailed discussion and comparison of the synthetic methods proposed for the production of Au NCs is beyond the purposes of this microreview; nevertheless, considered that the synthetic pathway plays a fundamental role in determining the photophysical properties of the resulting materials, we will briefly discuss this aspect in the present section. In particular we will focus on those approaches that demonstrated to produce quite monodisperse NCs. An exhaustive critical analysis of the possible strategies for Au NCs preparation can be found in recent review articles.[7a,14a–14d]

2.1 Synthesis of $Au_n(GS)_m$ NCs

Bottom-up (chemical) approach to Au NCs has been recognized to guarantee a good control on particle size and mono-dispersity.[14b,14d,16] Reduction of gold ionic species (e.g. Au^{III} in the form of $AuCl_4^-$) in the presence of thiols as stabilizer had been first proposed by Brust and Shiffrin for the synthesis of Au NPs in a two-phase liquid system using tetraoctylammonium bromide (TOAB) as a phase-transfer agent.[19] The groups of Whetten and Murray greatly contributed to optimize the process in order to decrease the size of the particles and improve structural control.[9,20] As schematized in Figure 2, in the first step (i) a large excess of thiol (molar ratio at least 3:1 with respect to gold) converts Au^{III} into Au^{I}–SR polymers. We would like to stress that according to recent investigation these polymeric motifs are partially maintained in the final NCs structure and they are considered to play a major role in determining the PL properties of the NCs and in particular their PL QY. Au^{I}-thiolate polymers are hence reduced to give Au^0 using a large excess of reductant (e.g. 10 equiv. of $NaBH_4$, stage ii in Figure 2).[18]

Despite such an excess of reducing agent the reaction is not complete and the presence of residual Au^{I} atoms in the NCs surface is fundamental both in conferring adequate chemical stability and in determining the optical and PL properties. In 2005, Negishi et al. produced and characterized a consistent series (summarized in Figure 3) of glutathione (GS) stabilized atomically precise Au NCs in homogeneous (methanol) solution.[21] Au NCs with different sizes were isolated by polyacrylamide gel electrophoresis (PAGE). Chemical compositions of the fractionated clusters determined electrospray ionization (ESI) mass spectrometry: $Au_{10}(SG)_{10}$, $Au_{15}(SG)_{13}$, $Au_{18}(SG)_{14}$,

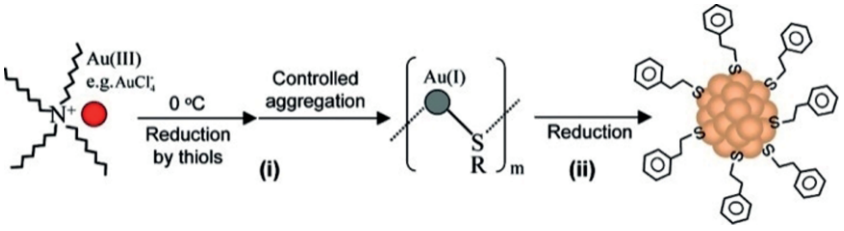

Figure 2. Scheme of the synthesis of Au NCs. In the first stage (i) Au-thiolate oligomers are formed. In a second step (ii) the oligomers are reduced to give the Au NCs. Reprinted with kind permission of the American Chemical Society from ref.[18]

Table 1. Photophysical properties of $Au_n(SG)_m$ NCs.[21]

Formula	Yield [mol-%]	ε/first peak [M^{-1} cm^{-1}]/[nm]	Emission maximum [eV]	PL QY[b]
$Au_{10}(SG)_{10}$, $Au_{11}(SG)_{11}$, $Au_{12}(SG)_{12}$	21[a]	1.1×10^4/330	1.5/3.0	1×10^{-4}/ 8×10^{-6}
$Au_{15}(SG)_{13}$	12	1.2×10^4/370	1.5/2.9	2×10^{-4}/ 1×10^{-5}
$Au_{18}(SG)_{14}$	23	1.1×10^4/570	1.5	4×10^{-3}
$Au_{22}(SG)_{16}$	8	1.1×10^4/560	1.6	4×10^{-3}
$Au_{22}(SG)_{17}$	7	1.5×10^4/540	1.7	2×10^{-3}
$Au_{25}(SG)_{18}$	11	8.8×10^3/670	1.5	1×10^{-3}
$Au_{29}(SG)_{20}$	9	8.5×10^3/690	1.4	3×10^{-3}
$Au_{33}(SG)_{22}$, $Au_{35}(SG)_{22}$	3[a]	1.3×10^4/710	1.4	2×10^{-3}
$Au_{38}(SG)_{24}$, $Au_{39}(SG)_{24}$	6[a]	1.1×10^4/730	1.4	2×10^{-3}

$Au_{22}(SG)_{16}$, $Au_{22}(SG)_{17}$, $Au_{25}(SG)_{18}$, $Au_{29}(SG)_{20}$, $Au_{33}(SG)_{22}$, and $Au_{39}(SG)_{24}$ were identified. Optical absorption and PL properties of these au NCs are reported in Table 1 and represent an important reference in order to understand the huge improvement made in the last decade in producing highly bright PL Au NCs.

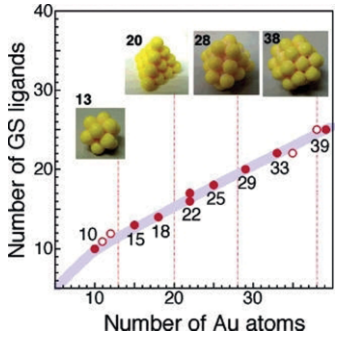

Figure 3. A plot of the chemical compositions of glutathione (GS) stabilized Au NCs prepared in ref:[21] reporting the number of Au atoms and GS ligands. The closed and open dots represent the most dominant and minor species contained in the fractions, respectively. The numbers depicted near the closed circles are the core sizes of the most dominant species. The models shown in the inset indicate the structures of highly symmetrical fcc crystals. Reprinted with kind permission of the American Chemical Society from ref.[21]

2.2 Size Focussing

Jin and co-workers notices the size-focusing phenomenon in their early work on the synthesis of $Au_{25}(SR)_{18}$ NCs, either in a two-phase[18] or a one-phase[22] approach. In those studies the first step, reduction of Au^{III} by excess thiol to form the Au^{I}/SR polymeric inter-mediate, was done at a low temperature (e.g., 0 °C) rather than at room temperature. After addition of $NaBH_4$ a gradual growth of monodisperse Au_{25} NCs from the size-mixed product was observed (Figure 4). This size-focusing growth process was found to be quite common (e.g., not limited by the type of thiol) and was demonstrated for other NC sizes [e.g. $Au_{38}(SR)_{24}$, $Au_{144}(SR)_{60}$].[22,23] The underlying principle of this size-focusing process is primarily related to the peculiar stability of certain sized $Au_n(SR)_m$ NCs: hence the key point to select size was to find the proper size distribution of the starting $Au_n(SR)_m$ mixture. The high yield of production of atomically defined Au NCs was further improved by the same authors by optimizing the solvent and using phenylethanthiol (HSC_2H_4Ph) as a ligand.

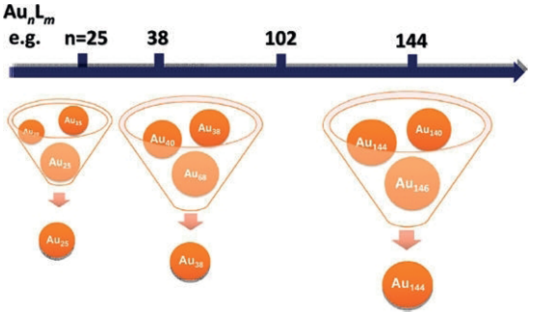

Figure 4. Schematization of the size focusing approach to the atomically controlled synthesis of Au NCs. Reprinted with kind permission of the American Chemical Society from ref.[23]

In particular the molecular $Au_{25}(SC_2H_4Ph)_{18}$ was produced in high yield and finally demonstrated to be suitable for crystallization. Determination of the X-ray structure of Au_{25}, and later of other NCs, represented a real innovation for understanding the origin of the PL of metal Au NCs since it allowed finally to correlate the optical and electronical features to structural ones.[41]

2.3 Mild Reductants and Etching

The use of mild reduction conditions has been proposed to achieve a better control on the size of Au NCs. In particular carbon monoxide has been proposed as a mild reducing agent to control and tune Au NCs size.[24] Reduction in alkaline conditions (NaOH) was also proposed as a size-control strategy in order to control the reducing activity of $NaBH_4$.[25]

2.4 Size Trasformation

Ligands-exchange is a versatile method to change the functionality and surface properties of NCs without changing the metal core structure.[26] Nevertheless, when NCs are treated in the presence of a large excess of thiol at suitably high temperature, ligand-exchange induced size/structure transformation (LEIST) occurs.[27] This process has been reported to be suitable to convert for example Au_{25} into Au_{28}, Au_{38} into Au_{36} and Au_{144} into Au_{133}.[27]

3. Structure of Au NCs

Crystallization and structural analysis of atomically precise Au NCs such as $Au_{25}(SR)_{18}$, $Au_{38}(SR)_{24}$ and $Au_{102}(SR)_{44}$,[20c,28] revealed the presence of a core-shell structure in which a highly symmetric Au^0 core (or kernel) is surrounded by a shell of staple like units with formula $SR–[Au^I–SR]_x$.

For example, Au_{25} cluster contains a centered icosahedral Au_{13} core (Figure 5, a), while the remaining twelve Au atoms are organized in an exterior hybrid shell which encapsulates also the eighteen thiolate ligands. All the thiolate ligands adopt a bridging bonding mode. Going more in detail, the external Au atoms are organized in six pairs of atoms interconnected to each other via a –SR ligand while two other –SR ligands interconnect them to the exterior Au atoms of the icosahedral core. Hence it is possible to identify 6 sub-structures containing two Au atoms and three –SR ligands that form an extended "staple" motif, where three sulfur and two gold atoms are arranged in a "V-shaped" –S–Au–S-Au–S– pattern. Each of this staple-like unit can be described with the formula Au_2SR_3 and the structure of $Au_{25}(SR)_{18}$ can be expressed as $Au_{13}@[Au_2(SR)_3]_6$.

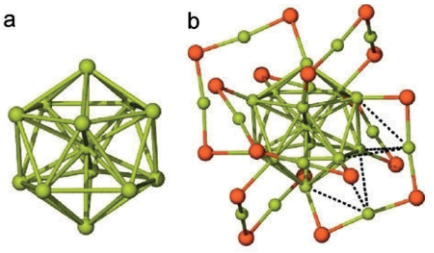

Figure 5. Example of the typical core-shell structure of thiolate stabilized Au NC. $Au_{25}(SR)_{18}$ contains a Au_{13} core (a) surrounded by a shell of staple-like units $Au_2(SR)_3$ as shown in (b). The formula of the NC can be also expressed as $Au_{13}@[Au_2(SR)_3]_6$. Reprinted with kind permission of the American Chemical Society from ref.[20c]

The structure of $Au_{38}(SC_2H_4Ph)_{24}$ is based upon a face-fused Au_{23} biicosahedral core, which is further capped by three monomeric $Au(SR)_2$ staples at the waist of the Au_{23} rod-like kernel and six $Au_2(SR)_3$ staples with three on the top icosahedron and other three on the bottom icosahedron (Figure 6). Because of the staggered configuration of the six dimeric staples the NC framework has a C_3 rotation axis.[29]

In the case of a cyclohexanethiolate-capped $Au_{23}(SR)_{16}^-$ nanocluster the structure comprises a cuboctahedron-based bipyramidal Au_{15} core, which is capped by two staple-like trimeric $Au_3(SR)_4$ units, two monomeric $Au(SR)_2$ and four plain bridging SR ligands.[30]

Larger NC as Au_{102} shows a more complicated structure that, still, can be known to atomic precision for the crystallized particles.[31] Nevertheless Salorinne et al. exploited a combination of multidimensional NMR methods, density functional theory calculations and molecular dynamics simulations to gain precise structural and dynamical information on the organic layer of this NC. The data evidenced disorder in the ligand organization and the presence of distinct ligand conformations of the most dynamic ligands.[32]

Structural information is fundamental to understand and model the optical properties of NCs. Although, even in the "static" picture gained by crystallographic data Au NCs presents

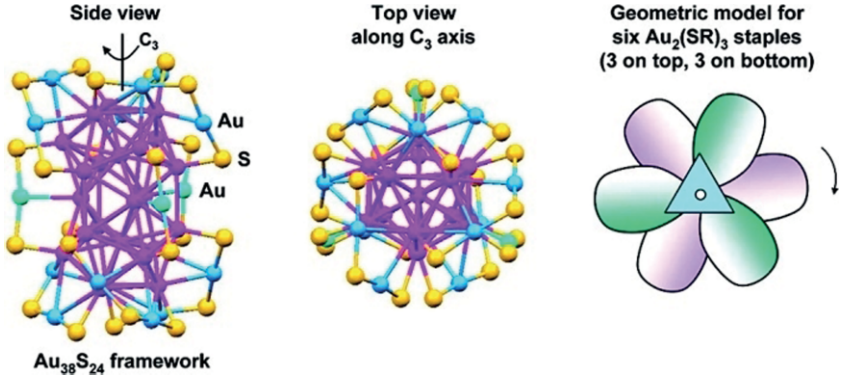

Figure 6. The structure of $Au_{38}(SC_2H_4Ph)_{24}$ is based upon a face-fused Au_{23} biicosahedral core and six $Au_2(SR)_3$ staples. Color labels: yellow, S; all the other colors are for Au atoms in different positions. The NC framework has a C_3 rotation axis. Reprinted with kind permission of the American Chemical Society from ref.[29]

quite a relevant complexity. Groups of gold atoms occupy non-equivalent positions in the structure (e.g. they are either part of the core or of the shell staple units), they have different electronic properties, and they are involved to a different extent in the interaction with the ligands. Different gold atoms hence are expected to give a different contribution in determining the NCs PL properties. The scenario becomes even more complicated when dynamical effects, related mostly to the ligands mobility, have to be taken into account as in the very relevant case of the interpretation of the PL of the NCs in solution.

4. UV/Vis Absorption of GNCs

As mentioned in section 1.2, absorption properties play a determinant role in the PL brightness. Differently from large NPs (diameter larger than 2 nm, that show a typical broad surface plasmon resonance band at ca. 2.4 ev in the absorption spectrum),[26b,34] Au NCs present molecular-like transition arising from efficient quantum effect.[14d] The absorption spectra of series of NC have been recently reviewed.[14d] The absorption spectrum of one of the most characterized and representative NC $Au_{25}(RS)_{18}^-$ is shown in Figure 7 where defined distinct absorption bands can be observed at 1.8, 2.75 and 3.1 eV.[18,33,35] Attribution of these transitions by Jim and co-workers was based on time-dependent density functional theory (TD-DFT) calculations[33] taking into account the structure obtained by X-ray crystallographic analysis (Figure 5).

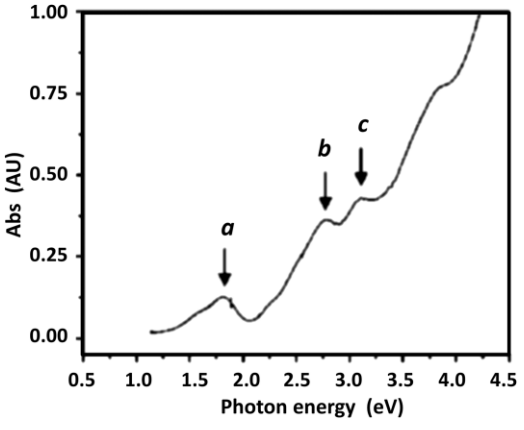

Figure 7. The UV/Vis spectrum of Au_{25} clusters (single crystals re-dissolved in toluene). Reprinted with kind permission of the American Chemical Society from ref.[33]

The results of the simulation are summarized in the electronic energy level diagram shown in Figure 8A. As shown in Figure 8B, the calculated absorption spectrum matches quite satisfactory the experimental one. In particular, the experimental peak at 1.8 eV (peak a in Figure 7) was interpreted essentially as an intraband (sp←sp) HOMO-to-LUMO transition.

Moreover, the HOMO and LUMO derive mainly from the combination of atomic orbitals of the 13 Au atoms in the icosahedral core rather than the 12 surface Au atoms. As a consequence the lowest energy optical absorption involve a transition localized on the Au_{13} core. Regarding the geometry of the

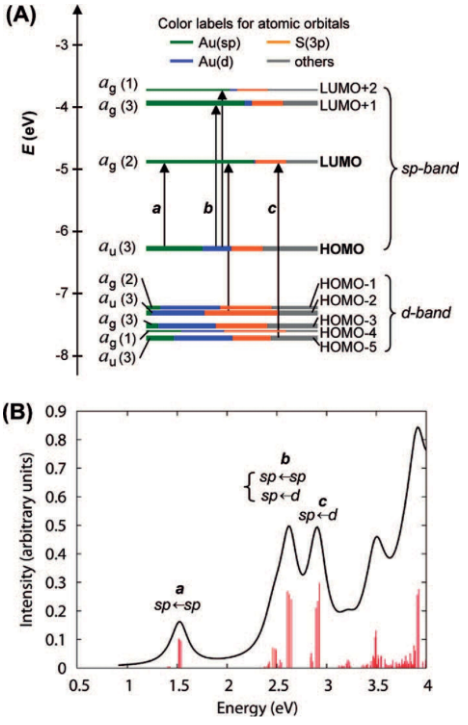

Figure 8. (A) Kohn–Sham (KS) orbital energy level diagram for a model compound $Au_{25}(SH)_{18}^-$. The energies are in units of eV. Each KS orbital is drawn to indicate the relative contributions (line length with color labels) of the atomic orbitals of Au (6sp) in green, Au (5d) in blue, S (3p) in yellow, and others in gray (those unspecified atomic orbitals, each with a < 1 % contribution). The left column of the KS orbitals shows the orbital symmetry (g, u) and degeneracy (in parenthesis); the right column shows the HOMO and LUMO sets. (B) The theoretical absorption spectrum of $Au_{25}(SH)_{18}^-$. Peak assignments: peak a corresponds to 1.8 eV, observed peak b corresponds to 2.75 eV (observed), and peak c corresponds to 3.1 eV (observed). Reprinted with kind permission of the American Chemical Society from ref.[33]

orbitals: the HOMO presents a two-lobe distribution of the electronic density similar to an atomic p orbital, while the LUMO exhibits d-like character. For this similarity of the molecular orbitals to atomic orbitals $[Au_{25}(SR)_{18}]^-$ can be viewed as a superatom,[14e] formally containing 8 valence electrons for the anionic cluster. Spin–orbit interaction (ignored in the simulate spectrum of Figure 8B) originates the splitting of the superatomic orbital set and the tail band observed in the experimental spectrum of Figure 7.[33,36]

The transitions at higher energy (b and c in Figure 7) arise from the occupied HOMO d band and they are interband (sp←d) transitions in the case of band c, whereas peak b is of mixed type. More detailed analysis was carried out by Aikens and co-workers.[37]

Discrete transitions were reported for $Au_{28}(SR)_{20}$[38] $Au_{36}(SR_{24})$[39] $Au_{38}SR_{24}$[40] boxes.[13] Similar analysis that allowed to correlate the absorption spectra to the X-ray crystallographic structures were performed for other atomic precise metal clusters Au_{20}[41,36] Au_{36}[42] Au_{18} and Au_{30}.[43]

A critical point in determining the actual brightness of gold NCs is the molar absorption coefficient. Indeed few data are available in the literature.[44] Negishi et al.[21] measured the molar absorption coefficient of a series of several $Au_n(GS)_m$ NCs

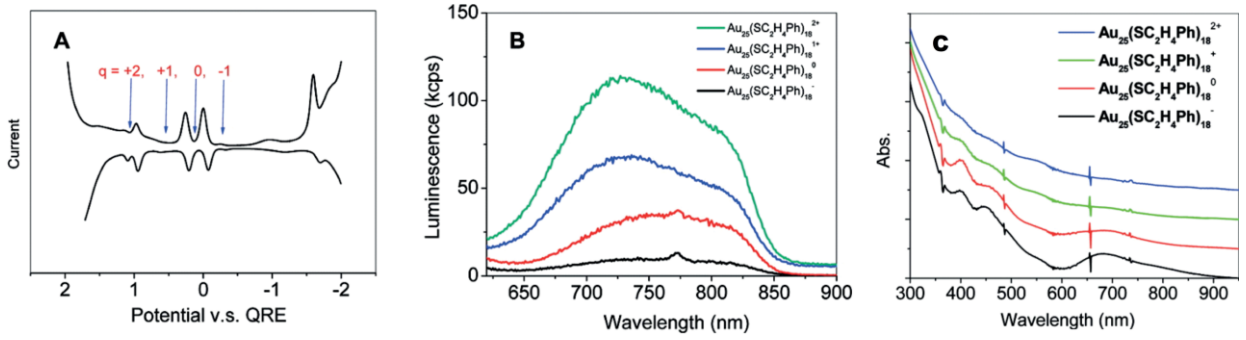

Figure 9. Charge states of $Au_{25}(C_2H_4Ph)_{18}$ probed by differential pulse voltammetry (DPV). (B) PL spectra of $[Au_{25}(C_2H_4Ph)_{18}]^q$ (q) –1, 0, +1, +2. (C) Comparison of the UV/Vis spectra of different charge states of Au_{25} species. For clarity, the spectra are vertically shifted. Reprinted with kind permission of the American Chemical Society from ref.[1]

after separation by PAGE. Although some of the fractions were not atomically pure ($n < 15$, $n > 29$) very interestingly these authors reported that, as shown in Table 1, independently on the size, the molar absorption coefficient is of the order of 10^4 $M^{-1}\,cm^{-1}$. The molar absorption spectrum of $Au_{25}(SC_2H_4Ph)_{18}$, reported more recently by Wang et al., confirmed these results.[45]

The position of the absorption peaks is, on the contrary, strongly size dependent and the lowest energy transition, in particular, it decreases its maximum wavelength upon decreasing the NC size as expected for quantum effect.

It is worth noticing that optimal organic dye with molar mass < 1 KDa show molar absorption coefficient as high as $1–2 \times 10^5$ $M^{-1}\,cm^{-1}$. In terms of brightness, this means that small Au NCs have, in general an absorption efficiency, which is one order of magnitude smaller than organic fluorophores. This is clearly a critical point in the design of ultra-bright gold NCs. A possible approach to face this drawback will be discussed in section 6.8.

For larger Au NCs, as the ubiquitous $Au_{144}(SCH_2CH_2Ph)_{60}$[46] (that still exhibit a stepwise, multiple-band absorption spectrum, indicating quantum confinement of electrons in the particle) a molar extinction coefficient 4×10^5 $M^{-1}\,cm^{-1}$ at 510 nm was reported. This value is considerably higher than what reported for smaller particles, nevertheless a significant contribution to light extinction due plasmon resonance as well as light scattering is expected considering the size of the NCs and actual absorption coefficient is expected to be much less. Absorption spectrum of Au NCs is strongly affected by the oxidation state.[1] As shown in Figure 9 the controlled oxidation of $Au_{25}(SC_2H_4Ph)_{18}^-$ up to $Au_{25}(SC_2H_4Ph)_{18}^{2+}$ causes a progressive loss of the band structure as well as a weakening of the absorbance.

5. Origin of the PL of Au NCs

In bulk conductive metals, valence electrons are free to move in the lattice through the conduction band. In the case of Au NCs, size of the metal starts to become comparable to the Fermi wavelength of an electron, and quantized electronic states[16,47] and energy levels start to emerge.[48] As a consequence, the most characteristic PL properties of Au NCs can be interpreted in terms of molecular orbitals and transitions between electronic states, analogously to what happens in molecules. For this reason, as anticipated in the previous sections, information about the actual structure of the NCs is essential for understanding and modeling[49] the electronic structure and the PL features.[14e,50] Both metal atoms and stabilizing ligands are expected to be involved in the electronic transition responsible for the PL emission to an extent that depends on their contribution to the HOMO–LUMO molecular orbitals. The typical core-shell structure of the Au NCs and the presence of staple-like motif suggested simplified interpretations where the emission is assumed to arise from a specific part of the NCs (e.g. either the inner Au atom kernel or the surface Au atoms actually interacting with the stabilizing ligand and at least in part in the Au^I oxidation state). This local origin of the PL and the identification of different "compartments" in the NCs contributed to understand the multiple emissions reported for Au NCs.

5.1 Effect of the Gold Core

A very simple theoretical model proposed to describe metal NCs PL is the Jellium model; it was adopted to account for size confinement quantum effects on metal NCs photophysical properties. Although this model is very simple and ignores the detailed structure of the NCs, it demonstrated, in some specific cases, a remarkable predicting power.[48b] It describes metal clusters valence electrons as confined in orbitals which have the same symmetry of the atomic ones and that are filled according to similar rules. The Jellium model predicts the scaling of spherical metal NCs transitions energy, in function of their radius (Figure 10), according to the simple [Equation (1)], where h is the Planck constant, ω_0 is the frequency of the transition, E_f is the Fermi Energy of bulk gold, N is the number of metal atoms of the cluster, r_s is the Wigner–Seitz radius of the metal and R is the radius of the cluster.[48b,51]

$$\hbar\omega_0 \cong E_f N^{-\frac{1}{3}} = E_f r_s / R \quad (1)$$

The model was initially developed for gas phase metal cluster but its efficacy has been demonstrated also in solution

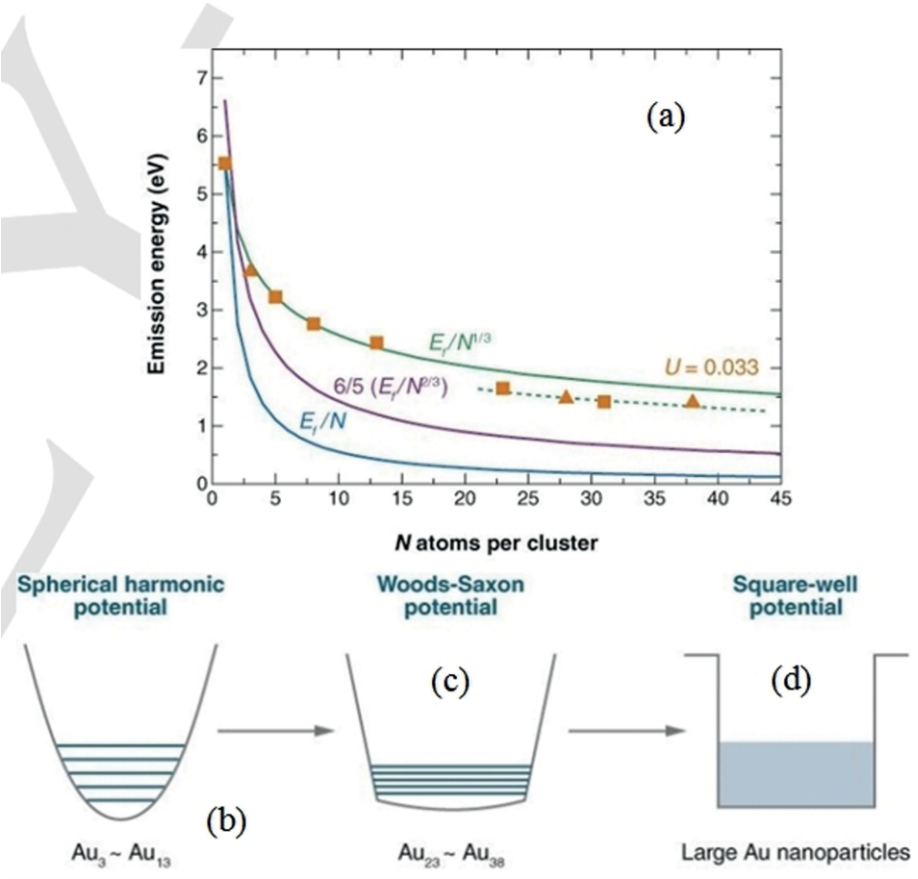

Figure 10. (a) correlation of the number of atoms (*N*) per cluster with emission energy as predicted by the jellium model (green line) for a harmonic potential (b). Kubo's model (blue line) and the square-potential-box model (purple line, potential d) do not match the experimental data. In the case of Au_{23} and Au_{31} slight deviations from the expected scaling can be corrected assuming a partially anharmonic potential (c). Reprinted with kind permission of the American Physical Society from ref.[48a]

phase by Zheng, Dickson and co-workers, who demonstrated that PAMAM dendrimer encapsulated Au NCs, with fewer than 40 atoms,[48a,48b] have both excitation and emission energies scaling as $E_f/N^{(1/3)}$. The Jellium model also predicts that when *N* increases, the spacing of the energy levels decreases, until it becomes smaller than k_bT, allowing plasmonic collective motions of the electrons.[48]

As mentioned, the Jellium model ignores the actual structure of the NCs and experimental data demonstrated that core size is not the only parameter that determines the PL properties of the Au NCs.

5.2 Effect of the Ligands and Au Oxidation State

Surface ligands have undoubtedly been proven to play a fundamental role in Au NCs PL.[53] This emerges clearly in the work of Wang et al., which showed that GNCs ranging from Au_{11} to Au_{201} and protected by different ligands, showed similar NIR emissions (Figure 11), which did not scale accordingly to their number of atoms.[52] The same group reported that this NIR emission intensity linearly increases with the fraction of polar thiolate introduced on the clusters surface by ligand exchange (conserving core sizes). In particular, they showed that the PL enhancement was proportional to the electron withdrawing capability of the ligand inserted and to the charge shift of the cluster core toward more positive values.[54]

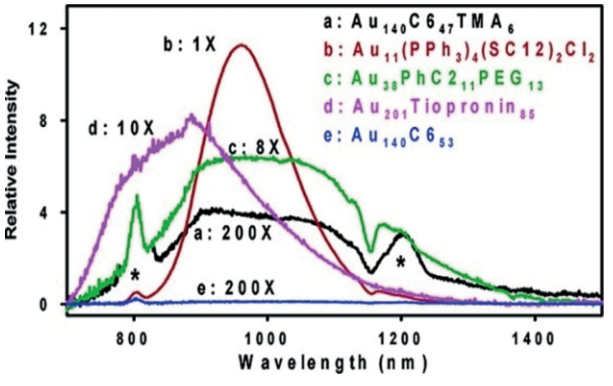

Figure 11. Au NCs with different core sizes and monolayers. C_6, C_{12},PhC_2, PEG, and PPh_3 represent hexanethiolate, dodecanethiolate, phenyl-ethanethiol, poly(ethylene glycol) (MW 350) thiolate, and triphenylphosphine, respectively. Reprinted with kind permission of the American Chemical Society from ref.[52]

Similar results have been reported by Wu and co-workers in the case of $Au_{25}(SR)_{18}$ NCs. These authors proved that changes

in the core charge state cause variations in the NIR PL QYs, excited state lifetimes and PL bands shape (Figure 9).[1] Recently, Crawford et al. reported the photophysical properties of aqueous, phosphine-terminated Au NCs after ligand exchange with a variety of sulfur-containing molecules.[53]

Prior to ligand exchange, the AU NCs showed no detectable PL, while after the introduction of sulfur-containing ligands PL initiates. The authors showed that small changes in sulfur substituents produce significant changes in the PL features including quantum yield, which ranges from 0.13 to 3.65 % depending on substituent (Figure 12). Going into detail, smaller ligands produce the most intense, highest energy, narrowest, and longest-lived emissions. Excited state lifetimes of these Au NCs varied to a large extent, from 59 to 2590 μs, demonstrating that even minor changes to the ligand substituent fundamentally alter the electronic properties of the NCs.

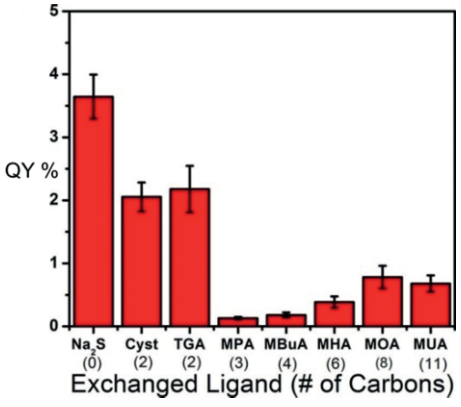

Figure 12. PL quantum yield plotted as a function of ligand chain length. Error bars represent the standard error across at least five independent trials. Reprinted with kind permission of the American Chemical Society from ref.[53]

The effect of Au^I content on the PL properties of Au NCs has been investigated in several studies.[55,56] Palmal and co-workers identified that Au NCs composed by only Au^0 have blue, green and yellow emission QYs in the order of 10 % and lifetimes in the order of nanoseconds, while the ones containing also Au^I have QY of 1 % and lifetimes in the order of microseconds.[56] Similar long luminescence decay components, in the order of the microsecond, are often observed in studies on Au NCs ligand dependent emissions.[57]

Oxidation of $Au_{25}(SG)_{18}$ by hydrogen peroxide does lead to significant enhancement of emission.[58] Slow oxidation was reflected in a gradual, time-dependent increase of PL. The PL intensity increased to the maximum, nearly 2.3-fold compared to the initial intensity. Of note, the addition of more excessive oxidant can accelerate the oxidation process, but it does not change the maximum emission intensity. This implies that the maximum emission relates to certain specific charge state(s) of Au_{25}.

5.3 Charge Transfer States

As discussed in the previous section, the effect of the nature of the stabilizing ligands on the PL properties of Au NCs is well documented and generally accepted. This effect was partially attributed to the polarity of the ligands, but different authors suggested that strong electronic coupling between gold atoms and ligand molecules originates charge transfer (CT) states where electrons are photo-injected form the ligands to the metal core. These CT states are analogous to the LMCT (ligand to metal charge transfer) or LMMCT (ligand to metal–metal charge transfer) transitions typical of metal complexes,[1] they affect the relaxation dynamic and their radiative deactivation produces PL.[53] In particular PL originated by CT state was observed for luminescent Au^I-thiolate monomeric species that constitute relevant simple models for the staple-like Au-thiolate oligomeric motif identified on the external structure of Au NCs.[1,59]

According to Jin and co-workers, formation of the CT state can occur according to two different mechanisms (Figure 13): (i) charge transfer from the ligands to the metal nanoparticle core through the Au–S bonds, and (ii) direct donation of delocalized electrons from electron-rich atoms or groups of the ligands to the metal core.

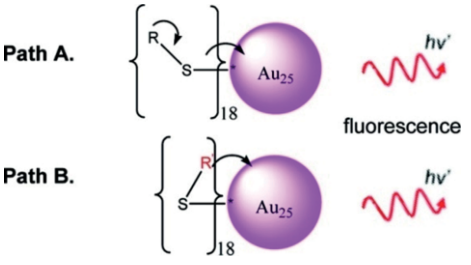

Figure 13. Mechanisms of formation of emissive LMCT states in Au NC. (A) charge transfer from the ligands to the metal nanoparticle core through the Au–S bonds, and (B) direct donation of delocalized electrons of electron-rich atoms or groups of the ligands to the metal core. Reprinted with kind permission of the American Chemical Society from ref.[1]

5.4 Aggregation

The CT emission observed for Au^I-thiolate monomers has been reported to be strongly affected by aggregation because of Au–Au interactions. Analogously, the oligomeric Au^I thiolate complexes,[59] typical precursors of Au NCs (Figure 2) have been demonstrated to show aggregation dependent PL.[14c,60] Luo and co-workers, in fact, found that glutathione gold thiolate polymers aggregation could be induced by solvent precipitation or by cation-induced aggregation, with the concomitant generation of strong microseconds lived luminescence.[60a] They identified this phenomenon as "aggregation induced emission" (AIE), by analogy with the behavior of other fluorophores classes.[2k] The emission of these aggregates have been hypothesized to be originated from a combination of Au···Au aurophilic interactions and LMCT (Figure 14).[1,60a,61] Aurophilic interactions in the aggregates depend on the thiolate polymer side chain nature and its electron withdrawing capability, which both have been proven to affect the optical properties of the system.[61]

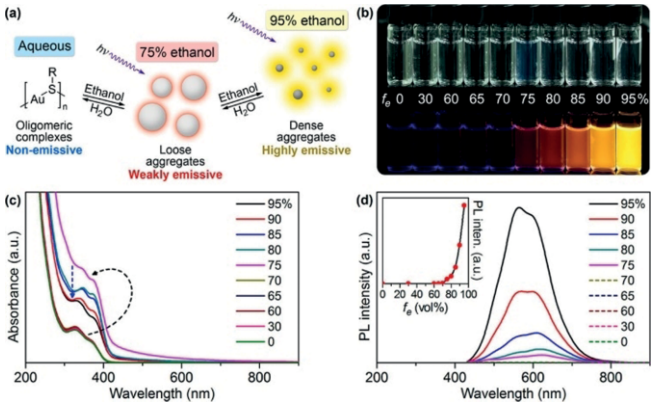

Figure 14. (a) Schematic illustration of solvent-induced AIE properties of oligomeric Au^{I}–thiolate complexes. (b) Digital photos of Au^{I}–thiolate complexes in mixed solvents of ethanol and water with different f_e under visible (top row) and UV (bottom row) light. (c) UV/Vis absorption and (d) photoemission spectra of Au^{I}–thiolate complexes in mixed solvents with different f_e. (Inset) Relationship between the luminescence intensity and f_e. The spectra were recorded 30 min after the sample preparation. Reprinted with kind permission of the American Chemical Society from ref.[60a]

5.5 Multiple Emission in GNCs

The presence of dual emission in Au NCs has been reported and investigated by Devades et al.[62] Ultrafast spectroscopic study on thiolate protected $Au_{25}(SR)_{18}$ clusters revealed the presence of two different emissions occurring simultaneously in the red and NIR region (Figure 15). The authors of this study suggested that the 500 nm emission fundamentally arises from the electron–hole recombination in the Au_{13} kernel with little perturbation from surface ligands, but the NIR emission at 700 nm originates from the recombination of holes in the ground core state and electron decay from core excited states to S–Au–S–Au–S semi rings, as schematized in Figure 16.[62]

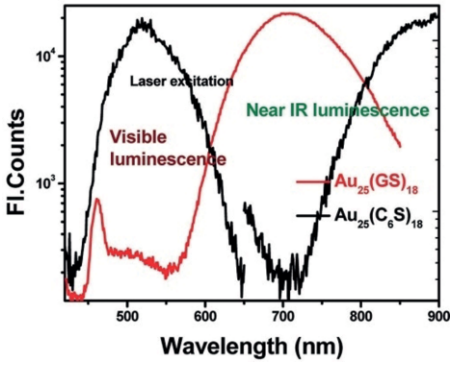

Figure 15. Luminescence spectra of Au_{25} clusters capped with C_6S and GS in DCM and water, respectively. Reprinted with kind permission of the American Chemical Society from ref.[62]

It is interesting to note that these semi-rings resemble the Au^{I}-thiolate structures at the basis of the AIE mechanism. Core transitions are short lived (tens of femtoseconds for few nanometers sized nanoparticles while surfaces transitions are long lived, in the order of microseconds).[63] Because of their nature long lived NIR emissions are commonly considered more sensible to Au oxidation state and to the ligands nature.[47,62,64]

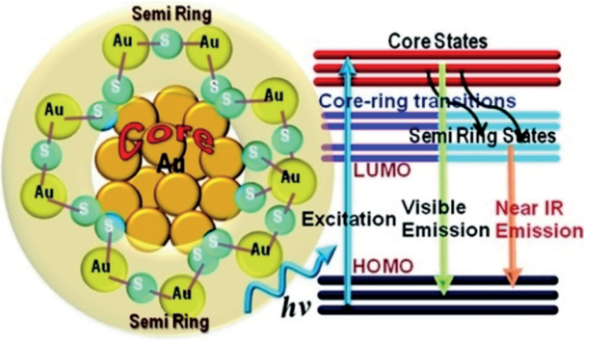

Figure 16. Electronic states and transitions responsible for the dual emission of Au_{25} clusters. Reprinted with kind permission of the American Chemical Society from ref.[62]

Wen et al. found that the far-red/NIR emission of BSA stabilized Au NCs is composed by two bands, one at 639 nm and the other at 704 nm which can be resolved by lowering the temperature. These two overlapped bands showed opposite peak shifts and bandwidth variations upon temperature changes, which suggest a different nature. Furthermore, luminescence lifetimes of this system measured at 600 nm showed two decay components, one of 3.2 ns and another of 1.5 μs.[65] These two bands have been attributed to prompt fluorescence and delayed fluorescence resulting from efficient ISC and thermally activated reverse ISC, between a singlet and a triplet states whose populations are in thermal equilibrium.[57]

6. Improving Brightness of GNCs

First reports about the PL of Au NCs revealed very low PL quantum yield (typically below 0.1 %) and hence a brightness too low for practical application in bio-imaging and bio-sensing.[21,54,66] As a consequence, for long time Au NCs have been considered as very efficient quenchers of the fluorescence of other organic and inorganic fluorophores rather than actual photo-luminescent probes. A big effort has been done by several research groups to enhance the brightness of Au NCs mostly by improving the PL quantum yield.[14d]

6.1 Au Clusters with Few Atoms

PL is a property of small metal NPs and very small,[12b] few-atoms NCs have been reported to show very high PL QY. In particular the Dickson' s group reported QY as high as 70 % for Au_5 and 42 % for Au_8 water-soluble, monodisperse, blue-emitting nanodots when they are encapsulated and stabilized by biocompatible poly(amidoamine) (PAMAM) dendrimers.[48a] Although the authors demonstrated the formation of the encapsulated nanocluster sizes with electrospray ionization (ESI) mass spectrometry, the actual origin of the observed PL has been debated,[67] since a similar emission was reported for PAMAM after oxidative treatment even in the absence of gold atoms[67].

6.2 Dithiolate Ligands

One order of magnitude enhancement of the near IR PL QY of Au_{25} monolayer protected clusters stabilized by phenylethanethiolate was reported upon ligand exchange with 1,4-dithiol durene.[69] Interestingly, a progressive decrease of the typical absorption band of the Au_{25} NCs was observed during the ligand exchange reaction.

A similar approach based on the use of lipoic acid derivatives was proposed by Aldeek and co-workers.[70] They developed a methodology to create clusters which can be functionalized with controllable amounts of different surface ligands. Their procedure allowed to synthesize ≈ 1.2 nm red emitting Au NCs, with emission QY between 10 % and 14 %, using different derivatives of lipoic acid.[69] By simply varying the ratio between these derivatives it has been possible to obtain clusters with a controlled amount of different ligands. Recently silane ligands have also been proposed to control the spectral and PL properties of Au NCs but the maximus achieved QY = 3.7 % was quite modest.[71]

6.3 Oxidative and Thermal Treatments

Controlled oxidation[72] has been reported to be beneficial for improving the PL QY of Au NCs. Figure 9 clearly shows an increase in the PL intensity of $Au_{25}(SC_2H_4Ph)_{18}^-$ upon increasing the oxidation state up to $Au_{25}(SC_2H_4Ph)_{18}^{2+}$. Oxidation of the lipoic acid ligands on Au_{22} NCs was also found to cause an enhancement of the quantum efficiency of their near-infrared luminescence to ca. 10 % (about 10 times relative increase). The produced nanocluster molecules contain 24 sulfur atoms, of which 6 of the outer sulfur atoms being oxidized into SO_3 species and another 18 forming classic Au–S bonding.[72] It is worth noticing that according to the authors oxidation occurs spontaneously in air during the purification process by dialysis.

Conroy et al. reported a five- to tenfold enhancement of near IR luminescence from monothiolate protected Au NCs after heating the particles in the presence of excess ligand thiols.[73] A final 5–10 % PL quantum efficiency was achieved for the emission in the 700–900 nm range. The effectiveness of this heating procedure was demonstrated for Au nanoclusters synthesized under a variety of conditions using two types of monothiols: mercaptosuccinic acid and tiopronin. We would like to underline that these thermal treatments, carried out in the presence of an excess of ligand causes a non-completely controlled etching of the NCs and hence a structural modification and the possible loss of the mono-dispersity of the sample.

6.4 Rigidification

According to Lee and co-workers, rigidification of the Au^I-thiolate shell of Au NCs has an outstanding effect on the PL efficiency and it may become a general effective strategy to enhance the photoluminescence efficiencies of gold clusters (Figure 17).[68] These authors reached this conclusion after investigating time-resolved and temperature-dependent luminescence properties of $Au_{22}(SG)_{18}$ NCs. They, in fact, observed a drastic increase of the visible luminescence quantum yield of the NCs below solvent freezing temperature and they concluded that shell rigidity enhances the luminescence quantum efficiency. Interestingly $Au_{22}(SG)_{18}$ NCs present a relevant QY (≈ 8 %) even in the absence of rigidification[74] because of AIE. In order to achieve rigidification of the gold shell at room temperature in fluid solution, $Au_{22}(SG)_{18}$ NCs were bound to the lipophilic bulky tetraoctylammonium (TOA) cations. Upon extraction in toluene, clusters with a PL QY greater than 60 % were obtained.

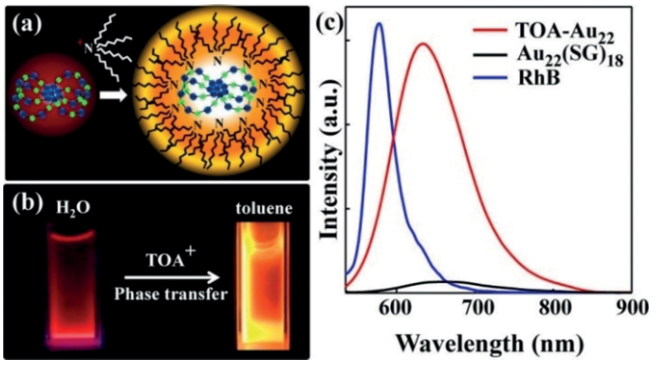

Figure 17. (a) Schematic of binding TOA to Au22$(SG)_{18}$ clusters (Au, blue; S, green), (b) digital photograph of $Au_{22}(SG)_{18}$ in water and TOA–Au_{22} clusters in toluene under long-wavelength UV lamp irradiation (365 nm), and (c) luminescence spectra of $Au_{22}(SG)_{18}$ in water and TOA–Au_{22} in toluene. Also, shown in the graph is the fluorescence spectrum of Rhodamine B (RhB, QY = 31 %) with the same optical density. Reprinted with kind permission of the American Chemical Society from ref.[68]

More recently, the same group prepared highly luminescent $Au_{22}(SG)_{18}$ clusters, by covalently modifying the ligands shell with small aromatic molecules and pyrene chromophores (Figure 18). This functionalization led to a fivefold PL enhancement after rigidifying the shell–gold structure. In this way highly luminescent water-soluble gold clusters with a PL quantum yield of 30 % were obtained at room temperature.[75] In this case, in combination with the rigidification effect, a contribution to the increase of the PL intensity due to excitation energy transfer

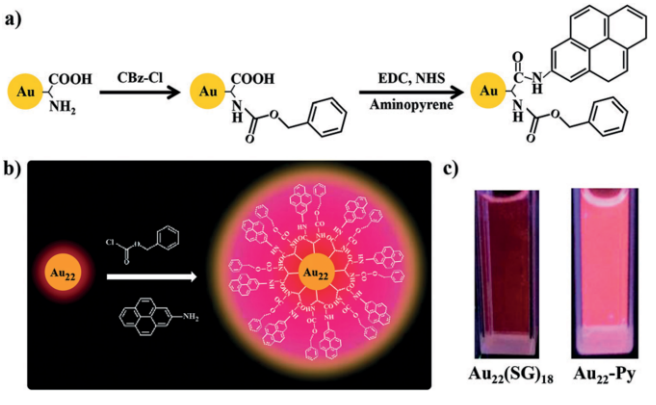

Figure 18. (a) CBz and pyrene functionalization procedure of Au_{22} clusters and (b) schematic diagram of CBz and Py functionalized $Au_{22}(SG)_{18}$ clusters (Au_{22}-Py). The digital photograph of Au_{22} and Au_{22}-Py clusters under long-wavelength UV lamp irradiation (365 nm). The optical densities of both clusters were 0.03 at 520 nm. Reprinted with kind permission of the Royal Society of Chemistry from ref.[75]

from the pyrene ligands to the metal core was observed, as discussed in section 6.8.

6.5 Protein Template

The use of proteins as template for the direct synthesis of Au NCs have been demonstrated to be very effective for producing particles with PL QY of about 10 % (hence several fold higher than their monolayer protected counterparts) and tunable excitation/emission spectral features.[76,77] Reaction conditions for protein-Au NCs production are very mild and environmental friendly. As additional advantages protein protected Au NCs present stable luminescence in a broad pH range (3–12) and in high ionic strength media. Moreover, the presence of biomolecular shell confers to these Au NCs a superior biocompatibility as well as a good colloidal stability and solubility in biological systems. In some applications these hybrids can also mimic bioactivity of natural proteins or be modified with functional groups which are specific for biological detection.

Xie et al. first reported in 2009 the use of bovine serum albumin (BSA) as the model protein for the templated synthesis of luminescent Au NCs.[78] BSA is the most abundant plasma protein widely used in applications such as sensing, self-assembly, and imaging. The formation process of BSA stabilized gold nanoclusters (BSA-Au NCs) is schematized in Figure 19. Under basic conditions (NaOH solution, pH > 12.0), the BSA stabilized Au NCs were obtained by mixing the metal ion precursor with BSA at 37 °C. The color of the solution changed from light yellow to light brown, and then to deep brown. The reaction was completed in ca. 12 h, without the addition of any external reductant, as confirmed by time-course measurements of the PL of the system. According to the authors, the tyrosine residue in BSA plays a fundamental role in reducing Au^{3+} to Au^{+}, which then is sequestered and entrapped by thiol groups of the protein. The oxidation state of the Au NCs was determined by X-ray photoelectron spectroscopy (XPS) that demonstrated the presence of two distinct components centered at binding energies of 84.0 attributed to Au^0 and 85.1 eV, assigned to and Au^I. These results demonstrated that the protein was able to further reduce the Au atoms to Au^0 leaving a fraction of Au^I atoms as small as ca. 17 %. Interestingly in control experiments the addition of an extraneous reductant, $NaBH_4$, in the same reaction produced Au NCs with very weak red PL (QY ≈ 0.1 %).

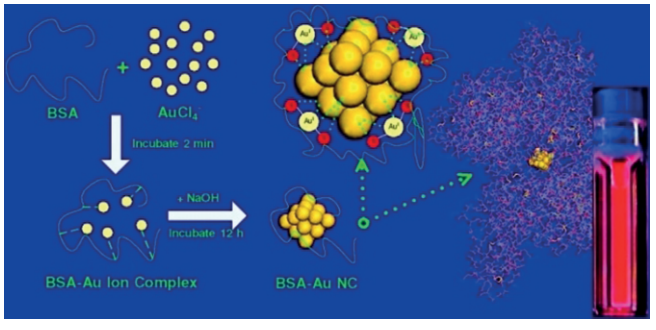

Figure 19. Scheme of the formation of BSA protected Au NCs. Reprinted with kind permission of the American Chemical Society from ref.[78]

TEM pictures of the BSA stabilized Au NCs (Figure 20) show particles with a size compatible with the one of Au_{25} ($d \approx 1.5$ nm) while, the same NPs, present a hydrodynamic diameter, measured by DLS (Figure 20), which is about 6 nm, similar to the size of the pristine BSA molecules. These results demonstrated that the encapsulation of Au NCs in BSA molecules has little effect on the structure of the BSA scaffolds.

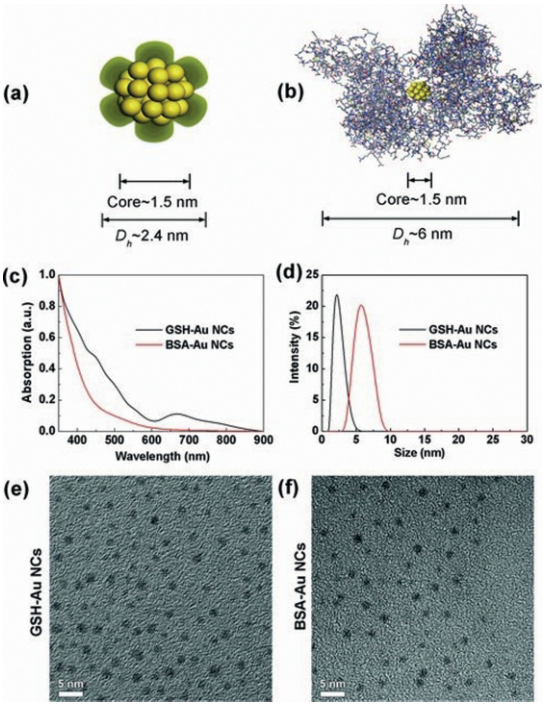

Figure 20. Schematic illustration of the core–shell structure of (a) GSH-Au_{25} NCs and (b) BSA-Au_{25} NCs. (c) UV/Vis and (d) DLS spectra of the as-prepared GSH-Au_{25} NCs (black line) and BSA-Au_{25} NCs (red line). Representative TEM images of the as-prepared (e) GSH-Au_{25} NCs and (f) BSA-Au_{25} NCs. Reprinted from ref.[77]

Recently, Guan and co-workers proposed a novel method for isolating BSA-protected Au_{25} clusters from free BSA[79] via co-precipitation with zinc hydroxide on their surface. The PL quantum yield slightly increases after purification by dialysis. Although the excitation and emission peaks at 480 and 640 nm, respectively, are compatible with the Jellium model, the absorption spectrum of the particles does not show the typical absorption band of thiolate stabilized Au_{25} and the spectrum profile suggests the presence of smaller clusters that may contribute significantly to the overall emission.

In fact, It has been shown that also Au_{20}[80] and Au_8[81] clusters can be synthesized inside BSA, and that clusters with different emission wavelength,[82] sizes and size distributions can be obtained with the same protein by changing pH, nature of the reductant, concentrations and temperature.[81–83]

After the demonstration of the ability of BSA to produce and protect Au NC, different investigators reported synthetic protocols based on alternative proteins as, for example, employing Insuline,[84] Lisozyme,[85] Apo-Ferritin,[86] Transferrine,[87] lactotransferrin (Lf),[88] DNase 1,[89] RNase-A,[90] Pepsine,[82] cytochrome c, myoglobin, milk holo α-lactalbumin (type I), milk β-lactoglobulin and pancreas α-chymotrypsin.[83]

Most of the proteins listed above, at basic pH, are capable of reducing gold to Au^0, with no need for additional reductants. This ability has been initially hypothesized to be due to the phenolic function of tyrosine, whose reducing power is enhanced above their pK_a.[78] Successive studies also identified a role of histidine showing that it can generate gold colloids when mixed with $HAuCl_4$ also in the absence of proteins.[86] Other accurate investigations on protein templated mineralization by mass spectrometry, XPS, photoluminescence and X-ray crystallography substantially confirmed the first findings and provided further details on its mechanism and kinetics.[91] Solid state experiments on protein single crystals[91a] showed the probable involvement of Au^I disproportion during the cluster growth as suggested for thiols directed synthesis with weak reducing agents.[56]

In another study, Volden et al. compared different proteins and they confirmed that the presence of thiolic amino acids function is not necessary for the formation and stabilization of GNCs in proteins. This group proposed a different generalized reaction mechanism in which anionic protein peptides play a fundamental function.[83]

In general, although the use of protein as template for the Au NCs synthesis is recognized as a versatile strategy for tuning PL spectral features and enhance their PL quantum yield, up to now the complex fundamental properties of protein-Au NCs, and in particular the origin of enhanced emission, have not yet been understood completely. A critical comparison of the optical absorption spectra, oxidative state and NCs size suggests the presence of different populations of Au clusters with different properties that can be hardly distinguished because of the complexity of the matrix. Unfortunately the protein shell that guarantees the stability and biocompatibility of the Au NCs, also prevents the possibility of isolating them. A further complication arises from quite modest yield of Au NCs production in the protein: a relevant fraction of the protein molecules does not incorporate gold particles.

6.6 Aggregation Effects

As shown in section 3, thiolate stabilized Au NCs present a core-shell structure in which the surface gold atoms are organized in staple-like motif with an oligomeric composition $Au_n(RS)_m$. These structures resemble those of small luminescent Au^I thiolate oligomeric complexes,[59] which emissions have been reported to be originated from LMCT[61] and LMMCT[1,60a] states and to be sensible to Au···Au aurophilic interactions. These aurophilic interactions depend on the thiolate side chain nature and its electron withdrawing capability, and they are strongly enhanced upon aggregation, enhancing the PL QY of Au-thiolate complexes.[60a,61] A similar effect was observed for the glutathione gold thiolate polymers precursors of Au NCs in their synthesis (Figure 2): upon aggregation, produced by solvent modification or the addition of suitable cations, a strong enhancement of the microseconds lived luminescence was reported (Figure 14).[60a] Luo et al. took advantage of this phenomenon to synthesize bright PL Au NCs with an high ratio Au^I/Au^0 and PL QYs around 15 %.[60a] The emission of these Au^0Au^I–SG NCs, prepared according to the Scheme shown in Figure 21, was found to be very similar to that observed for gold thiolate oligomers in terms of peaks position, shape, intensity and lifetime. For this reason, the authors suggested that the observed luminescence resulted from the AIE of Au^I thiolates on nanoclusters surface.[60a]

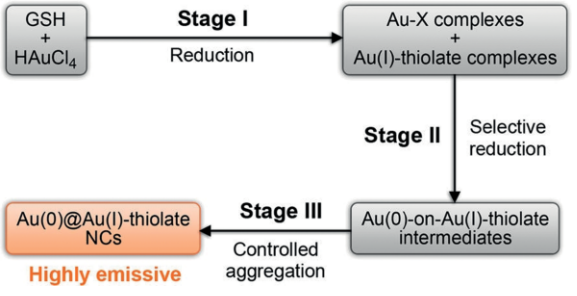

Figure 21. Schematic of synthesis of highly luminescent Au^0@Au^I–thiolate NCs. X in the Au^I–X complexes can be any non-thiolate functional group in the reaction mixture. Reprinted with kind permission of the American Chemical Society from ref.[60a]

Recently Yahia-Ammar et al. exploited AIE to develop a simple, fast, and robust protocol for the preparation of luminescent NPs of ca. 120 nm diameter resulting from the cationic polymer polyallylamine hydrochloride (PAH) mediated self-assembly of Au-GSH NCs.[92] These monodisperse and positively charged Au-GSH-PAH NPs showed a strong photoluminescence en-

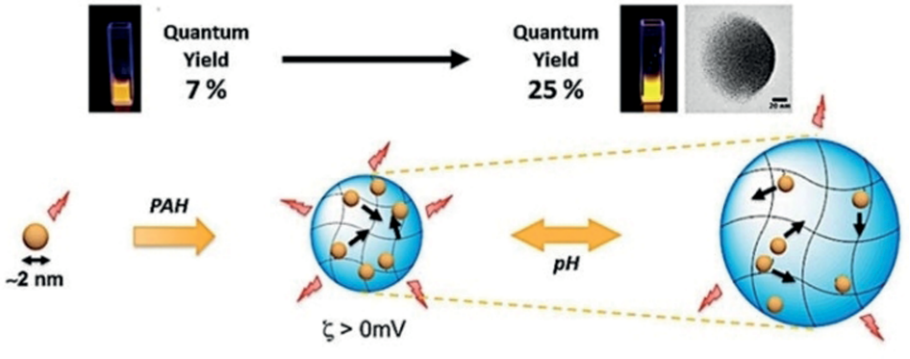

Figure 22. Scheme of the formation of Au-GSH-PAH NPs by self-assembly (bottom). The NPs swell upon increasing pH from 6 to 8. NPs self-assembly leads to an increase in the PL QY. Reprinted with kind permission of the American Chemical Society from ref.[92]

hancement to a PL QY of 25 %, pH-dependent swelling properties and excellent colloidal and photostability in water, buffer, and culture medium. Different Au NCs surface ligands and cationic polymers were investigated in order to demonstrate the versatility of this approach. The importance of the interaction between the NCs on the PL efficiency was demonstrated by steady-state and time-resolved measurements exploiting the pH-dependent swelling. DLS measurements demonstrated that, as shown in Figure 22, an increase of the pH led to a continuous shift of the mean particle size from 80 nm (at pH 6) to 350 nm (at pH 11), which is reversible by adjusting the pH in the range 6 to 10. The low polydispersity index obtained for each measurement (PDI < 0.2) suggests that the size increase is related to swelling of the self-assembled NP rather than their aggregation. The effect of pH on the PL intensity Au-GSH-PAH was investigated and it was found out that the swelling of the NPs caused a PL intensity decrease switching the pH from 6 to pH > 8.3 (which is the pK_a of PAH) due to the weak inter-NCs interaction that is associated with the particle swelling. Lowering the pH to 6.5 enabled recovery of the initial PL intensity confirming the reversibility of particle swelling.

6.7 Silver and Copper Doping

Partial replacement of the Au atoms in the NCs with silver has been reported to have a strong effect on the PL QY.[93] Wang et al. compared two series of Ag-doped $Ag_xAu_{(25-x)}$ nanoclusters, prepared by two different routes, and they reported a drastic PL enhancement for Au_{25} upon reaction with Ag^I thiolate, after the substitution of 13 Au atoms with Ag.[94] Interestingly, the mixed cluster $Ag_xAu_{(25-x)}$ with x < 13, showed only weak PL (QY ≈ 0.2 %). On the contrary, controlled reaction of Au_{11} clusters with Ag^I-thiolate produced the very bright luminescent (PL QY ≈ 40 %) $Ag_{13}Au_{12}$. Structural analysis shows that the $Ag_xAu_{(25-x)}$ nanoclusters are geometrically identical and that they adopt the same biicosahedral structure of Au_{25}. X-ray crystallography was used to determine the substitution sites of Ag atoms in the $Ag_xAu_{(25-x)}$ cluster, through partial occupancy analysis; this provided insight into the mechanism of photoluminescence enhancement.

In fact, the alloy cluster become highly fluoresce only when the 13 Au sites, that contribute with their atomic orbitals to the NC HOMO and LUMO, are fully substituted with silver. A complete change in the nature of the electronic states and orbitals involved in the transition responsible for the PL hence occurs upon replacing 13 gold atoms.

An alternative strategy to prepare bright PL Ag_xAu_y cluster is based on the modification of silver NCs. Soldan et al. reported[95] a 26 fold increase of the PL QY of an Ag_{29} NC by doping with a discrete number of Au atoms, producing $Ag_{(29-x)}Au_x$ with x = 1–5. As shown in Figure 23, the Au-doped clusters exhibit a strong red emission around 660 nm which is as more intense as higher is the number of gold atoms in the structure. A change of the nature of the HOMO and LUMO, and as a consequence of the electronic transitions responsible for the PL, was reported to be, also in this case, the reason of the enhanced QY in the alloy NCs.

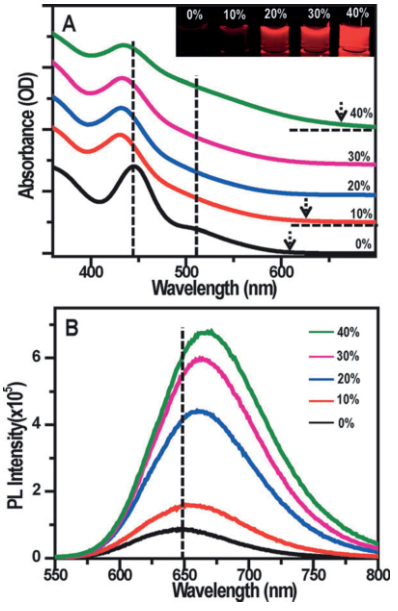

Figure 23. (A) UV/Vis and (B) PL spectra of Ag^{29} and Au-doped Ag^{29} clusters synthesized using different amounts (mmol-%) of Au. Inset: a photograph of Ag^{29} and Au-doped Ag^{29} clusters under a UV lamp (using 365 nm light). Reprinted from ref.[95]

Recently, it was reported that copper[96] can play a role similar to silver in enhancing the PL of Au NCs. Kang described the preparation and characterization of Au_2Cu_6 NCs constituted by six thiolated Cu atoms aggregated by two Au atoms that show a quantum yield of 11.7 %.[97]

In conclusion, gold based alloy NCs, if properly designed, show a considerably high PL QY and may become suitable for bioimaging. The doping with metals less noble than gold such as silver and copper is certainly an advantage from the economical point of view. Nevertheless the actual stability of these mixed NCs and of their PL need further investigation.

6.8 Light Harvesting Ligands

Brightness of nanoprobes depends not only on the PL quantum yield but, strongly, on the efficiency of absorption of the excitation light (ε). As discussed in section 4, Au NCs present a molar absorption coefficient ($\varepsilon \approx 10^4$ M^{-1} cm^{-1}) which is about one order of magnitude lower than organic chromophores. In order to improve this feature, our and other groups proposed the design of hybrid structures that combine the PL properties of Au NCs with the optical properties of organic dyes in order to enhance the brightness of the inorganic emitters. A considerable improvement of brightness can in fact be achieved by introducing ligands able to efficiently adsorb light (chromophores) and to transfer the excitation energy to the emitting gold core.[98,99]

According to this strategy, we prepared Au_{101} NCs[100] stabilized with phosphine ligands terminated with a pyrene chromophores (Figure 24).[98] Absorption spectra of nanoparticles are dominated by the contributions of the pyrene chromophores in the UV regions and are almost coincident with the absorption spectrum of the NCs in the visible-NIR range. A partial broaden-

ing and bathochromic shift of the pyrene was observed upon binding to the NCs. An increase of brightness of about one order of magnitude was detected upon excitation of the organic chomophores demonstrating that excitation energy absorbed by the pyrene was transferred with high efficiency (> 95 %) to the Au NCs producing sensitized NIR emission (Figure 24). The occurrence of the efficient energy transfer (ET) process[101] was confirmed by the presence of the pyrene electronic transition peaks in the PL excitation spectrum of the Au NC. More detailed investigation revealed that the enhanced brightness was not only the effect of the ET process from the pyrene ligand to the gold but that also a large increase of the PL QY occurred because of the replacement of the simple triphenylphosphine with the pyrene terminated ligands.

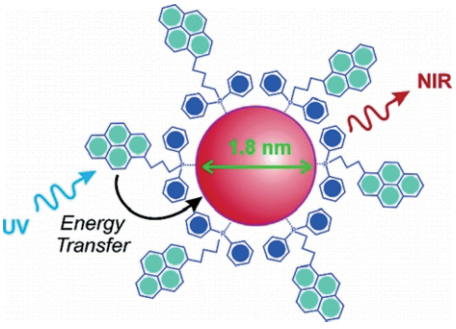

Figure 24. Scheme of a hybrid Au NCs functionalized with pyrene chromophores. The ligands absorb the excitation light very efficiently and they transfer the excitation energy to the Au core producing sensitized emission. The light-harvesting process increases the NCs brightness. Reprinted with kind permission of the American Chemical Society from ref.[98]

Pyo et al. recently investigated an analogous system having a pyrene terminated ligand bound to Au_{22} NCs (Figure 18).[75] The chromophores were expected to enhance the PL brightness of the Au NCs by excitation ET from pyrene to the Au_{22} NCs but, in this case, the energy transfer efficiency was found to be only 14 % because of the competing electron transfer deactivation pathway. Electron transfer in fact was evidenced by the formation of the pyrene anion radical revealed in ultrafast transient absorption measurements. Moreover, steady-state and time-resolved PL measurements have shown evidence of enhanced rigidity with increased PL lifetimes for the functionalized Au_{22} NCs.

To suppress the electron transfer pathway, the pyrene functionalized Au_{22} NCs were ion-paired with tetraoctylammonium (TOA) cations that could break the electron transfer pathway, leading to a dramatic 37-fold increase in PL brightness with the resonance energy transfer efficiency of ca. 80 %. This work demonstrated the possibility of combining multiple effects, in the specific case light-harvesting ligands and rigidifiaction, to enhance the PL brightness of gold NP.

More recently, we proposed a different strategy to turn on/off the PL of Au_{144} NCs using as organic sensitizer a photoswitchable azobenzene derivative (Figure 23).[99] The conversion of the *trans* form of the ligand into the *cis* one took place almost quantitatively (> 95 %) with a quantum yield identical to the one measured for the same molecule free in solution (upon irradiation at 360 nm). Regeneration of 70 % of *trans* was, in turn, achieved by irradiation of cA-GNP at 480 nm.

Photophysical results confirmed the occurrence of an excitation energy transfer process from the ligands to the Au NCs that produced sensitized NIR emission. Because of this process, the excitation efficiency of the gold core, upon excitation of the ligands, is much higher for the *trans* form than for the *cis* one (Figure 25). Moreover thanks to the ET process the PL brightness of the Au NCs is enhanced upon excitation of the ligands, both in the *cis* and *trans* form with respect to the bare NCs.

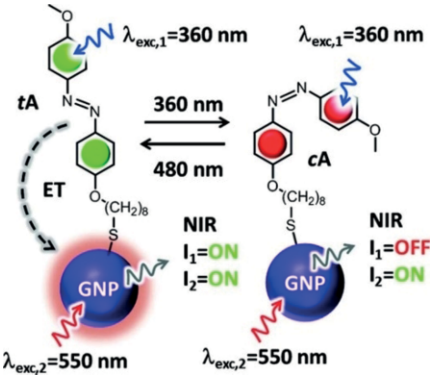

Figure 25. Chemical formula of the *trans* azobenzene tA and of its cisisomer cA bound to gold NP (GNP). When the ligands are in the *trans* form (left, tA-GNP, ON state) ET from tA to the GNP produces NIR-sensitized emission upon ligand excitation. Such contributions, owing to sensitization, are lost upon PI in cA covered NPs (right, cA-GNP, OFF state). Reprinted from ref.[99]

Interestingly, in these azobenzene functionalized Au NCs, the photo-isomerization rate of the ligands was not affected by the interaction with the gold NCs. This outcome demonstrated that excitation energy transfer to gold assists photo-isomerization, rather than competing with it.

7. Outlook and Conclusions

Recent developments in the design of PL Au NCs demonstrated that several approaches permit to enhance the initially reported poor brightness of these NPs. As far as the PL QY is concerned, in fact, values as low as 0.1–0.4 % were reported for a set of Au-GS NC and PL efficiency of this order of magnitude or even lower are typical of most Au NCs. Nevertheless, during last few years, examples of Au NCs with PL QY as high as 40–60 % have been reported. Most promising applications of these materials is surely in bio-imaging. In this context, the actual chemical and photochemical stability of Au NCs in biological media is still a relevant issue, although their applicability as PL contrast agent has been demonstrated both in vitro and in vivo.[10]

Synthesis of Au NCs using proteins as template represented a real advance in the search of bright PL inorganic nanoprobes since it allowed the preparation of NCs with acceptable QY (≈ 10 %), tunable excitation/emission spectral features, high bio-compatibility and resistance to changes in pH and ionic strength. Nevertheless, the protein templating action is not suitable to prepare pure, clearly monodisperse Au NCs since the removal of the biomolecular shell and the isolation of the incorporated NCs in a non-invasive way is still not possible. Moreover

because of the poor efficiency of the NCs production a large amount of NC-free protein is present at the end of the synthesis and methods proposed to remove such an excess strongly alter the structure/composition of the NCs. As a consequence, the detailed characterization of the Au NCs obtained by protein template, that would require the isolation of all the representative gold species from the biomolecular matrix, is not possible and the complex fundamental properties of protein-Au NCs, and in particular the origin of enhanced emission, has not yet been understood completely.

Also the control of chemical and physical parameters such as NCs size, ligands nature and polarity, temperature and oxidation state, demonstrated to be a powerful strategy to devise bright PL Au NCs. In addition, controlled replacement of Au atoms with other metal, and especially silver was proved to yield very bright NPs. Nevertheless, it is well known that Au NCs structure and composition may evolve, relatively fast, especially in solution, and processes like core etching or fission, ligand exchange or metal oxidation can occur in an uncontrolled way especially in a potential biological matrix. Hence all the NCs with unusual composition (e.g. alloy NCs) or prepared under unusual conditions (e.g. high temperature or oxidative environment) are expected to evolve towards more stable forms, and to lose, at least potentially, their high brightness. Hence actual stability of these "exotic" NCs and of their PL needs further investigation.

Aggregation and rigidification based approaches are, up to now, the most promising for producing Au NCs with PL quantum yields as high as 40–60 %. Although AIE and rigidification effect are clearly distinguished by most authors, detailed photophysical investigation revealed quite a complex scenario where the two mechanisms can be only in part discriminated.

Despite its importance, the need of an efficient absorption of the excitation energy for the development of ultra-bright Au NCs has been ignored to a large extent. We believe that improving the typically low molar absorption coefficient of Au NCs is indeed a major challenge and we proposed the use of light harvesting ligands for capturing light with high efficiency and transferring the excitation energy to the Au NCs. We believe that the combination of this approach with the previously discussed strategy aiming to enhance the NC PL QY will pave the road to hybrid ultra-bright NPs that will match the best properties of organic and inorganic nanomaterials to give innovative PL probes for bio-applications.

Acknowledgments

We gratefully acknowledge financial support from the European Research Council (ERC) ("MOSAIC" Starting Grant 259014) and the US Army Research Office (US-ARO) project W911NF-16-1-0324.

Keywords: Gold · Nanoparticles · Fluorescence · Photoluminescence · Nanoclusters

[1] Z. Wu, R. Jin, *Nano Lett.* **2010**, *10*, 2568–2573.
[2] a) Y. Jin, *Acc. Chem. Res.* **2014**, *47*, 138–148; b) H. Liang, X.-B. Zhang, Y. Lv, L. Gong, R. Wang, X. Zhu, R. Yang, W. Tan, *Acc. Chem. Res.* **2014**, *47*, 1891–1901; c) K. Li, B. Liu, *Chem. Soc. Rev.* **2014**, *43*, 6570–6597; d) H. Xu, Q. Li, L. Wang, Y. He, J. Shi, B. Tang, C. Fan, *Chem. Soc. Rev.* **2014**, *43*, 2650–2661; e) K. Yang, L. Feng, X. Shi, Z. Liu, *Chem. Soc. Rev.* **2013**, *42*, 530–547; f) B. H. Kim, M. J. Hackett, J. Park, T. Hyeon, *Chem. Mater.* **2014**, *26*, 59–71; g) L. Zhang, E. Wang, *Nano Today* **2014**, *9*, 132–157; h) L. Zhang, W.-F. Dong, H.-B. Sun, *Nanoscale* **2013**, *5*, 7664–7684; i) M. Montalti, L. Prodi, E. Rampazzo, N. Zaccheroni, *Chem. Soc. Rev.* **2014**, *43*, 4243–4268; j) E. Rampazzo, F. Boschi, S. Bonacchi, R. Juris, M. Montalti, N. Zaccheroni, L. Prodi, L. Calderan, B. Rossi, S. Becchi, A. Sbarbati, *Nanoscale* **2012**, *4*, 824–830; k) M. Montalti, G. Battistelli, A. Cantelli, D. Genovese, *Chem. Commun.* **2014**, *50*, 5326–5329; l) N. T. K. Thanh, N. Maclean, S. Mahiddine, *Chem. Rev.* **2014**, *114*, 7610–7630; m) M. Montalti, A. Cantelli, G. Battistelli, *Chem. Soc. Rev.* **2015**, *44*, 4853–4921; n) C. Caltagirone, A. Bettoschi, A. Garau, R. Montis, *Chem. Soc. Rev.* **2015**, *44*, 4645–4671.
[3] a) A. S. Klymchenko, *Acc. Chem. Res.* **2017**, *50*, 366–375; b) M. T. Proetto, C. R. Anderton, D. H. Hu, C. J. Szymanski, Z. H. Zhu, J. P. Patterson, J. K. Kammeyer, L. G. Nilewski, A. M. Rush, N. C. Bell, J. E. Evans, G. Orr, S. B. Howell, N. C. Gianneschi, *ACS Nano* **2016**, *10*, 4046–4054.
[4] a) Q. Zheng, M. F. Juette, S. Jockusch, M. R. Wasserman, Z. Zhou, R. B. Altman, S. C. Blanchard, *Chem. Soc. Rev.* **2014**, *43*, 1044–1056; b) E. M. S. Stennett, M. A. Ciuba, M. Levitus, *Chem. Soc. Rev.* **2014**, *43*, 1057–1075; c) A. P. Blum, J. K. Kammeyer, A. M. Rush, C. E. Callmann, M. E. Hahn, N. C. Gianneschi, *J. Am. Chem. Soc.* **2015**, *137*, 2140–2154.
[5] a) E. S. Shibu, M. Hamada, S. Nakanishi, S. Wakida, V. Biju, *Coord. Chem. Rev.* **2014**, *263*, 2–12; b) I. J. Kramer, E. H. Sargent, *Chem. Rev.* **2014**, *114*, 863–882; c) J. B. Blanco-Canosa, M. Wu, K. Susumu, E. Petryayeva, T. L. Jennings, P. E. Dawson, W. R. Algar, I. L. Medintz, *Coord. Chem. Rev.* **2014**, *263*, 101–137; d) G. Y. Fan, C. Y. Wang, J. Y. Fang, *Nano Today* **2014**, *9*, 69–84; e) P. Wu, X. P. Yan, *Chem. Soc. Rev.* **2013**, *42*, 5489–5521; f) P. Zrazhevskiy, M. Sena, X. H. Gao, *Chem. Soc. Rev.* **2010**, *39*, 4326–4354; g) F. Pinaud, S. Clarke, A. Sittner, M. Dahan, *Nat. Methods* **2010**, *7*, 275–285; h) I. L. Medintz, H. T. Uyeda, E. R. Goldman, H. Mattoussi, *Nat. Mater.* **2005**, *4*, 435–446; i) Y.-P. Ho, K. W. Leong, *Nanoscale* **2010**, *2*, 60–68; j) U. Resch-Genger, M. Grabolle, S. Cavaliere-Jaricot, R. Nitschke, T. Nann, *Nat. Methods* **2008**, *5*, 763–775.
[6] a) K. M. Tsoi, Q. Dai, B. A. Alman, W. C. W. Chan, *Acc. Chem. Res.* **2013**, *46*, 662–671; b) K. M. Tsoi, S. A. MacParland, X. Z. Ma, V. N. Spetzler, J. Echeverri, B. Ouyang, S. M. Fadel, E. A. Sykes, N. Goldaracena, J. M. Kaths, J. B. Conneely, B. A. Alman, M. Selzner, M. A. Ostrowski, O. A. Adeyi, A. Zilman, I. D. McGilvray, W. C. W. Chan, *Nat. Mater.* **2016**, *15*, 1212–1221.
[7] a) Y. Tao, M. Li, J. Ren, X. Qu, *Chem. Soc. Rev.* **2015**, *44*, 8636–8663; b) L.-Y. Chen, C.-W. Wang, Z. Yuan, H.-T. Chang, *Anal. Chem.* **2015**, *87*, 216–229.
[8] X. Yang, M. X. Yang, B. Pang, M. Vara, Y. N. Xia, *Chem. Rev.* **2015**, *115*, 10410–10488.
[9] T. Huang, R. W. Murray, *J. Phys. Chem. B* **2001**, *105*, 12498–12502.
[10] A. Cantelli, G. Battistelli, G. Guidetti, J. Manzi, M. Di Giosia, M. Montalti, *Dyes Pigm.* **2016**, *135*, 64–79.
[11] a) G. Battistelli, A. Cantelli, G. Guidetti, J. Manzi, M. Montalti, *Wiley Interdiscip. Rev. Nanomed. Nanobiotechnol.* **2016**, *8*, 139–150; b) A. Reisch, A. S. Klymchenko, *Small* **2016**, *12*, 1968–1992.
[12] a) M. Hesari, Z. F. Ding, *Acc. Chem. Res.* **2017**, *50*, 218–230; b) L. Wu, W. Fang, X. Chen, *Phys. Chem. Chem. Phys.* **2016**, *18*, 17320–17325; c) K. L. D. M. Weerawardene, C. M. Aikens, *J. Am. Chem. Soc.* **2016**, *138*, 11202–11210; d) Z. Gan, Y. Lin, L. Luo, G. Han, W. Liu, Z. Liu, C. Yao, L. Weng, L. Liao, J. Chen, X. Liu, Y. Luo, C. Wang, S. Wei, Z. Wu, *Angew. Chem. Int. Ed.* **2016**, *55*, 11567–11571; *Angew. Chem.* **2016**, *128*, 11739.
[13] C. Zeng, Y. Chen, K. Iida, K. Nobusada, K. Kirschbaum, K. J. Lambright, R. Jin, *J. Am. Chem. Soc.* **2016**, *138*, 3950–3953.
[14] a) H. L. Li, W. L. Zhu, A. J. Wan, L. B. Liu, *Analyst* **2017**, *142*, 567–581; b) R. Jin, C. Zeng, M. Zhou, Y. Chen, *Chem. Rev.* **2016**, *116*, 10346–10413; c) N. Goswami, Q. F. Yao, Z. T. Luo, J. G. Li, T. K. Chen, J. P. Xie, *J. Phys. Chem. Lett.* **2016**, *7*, 962–975; d) R. Jin, *Nanoscale* **2015**, *7*, 1549–1565; e) H. Hakkinen, *Chem. Soc. Rev.* **2008**, *37*, 1847–1859; f) G. Battistini, P. G. Cozzi, J. P. Jalkanen, M. Montalti, L. Prodi, N. Zaccheroni, F. Zerbetto, *ACS Nano* **2008**, *2*, 77–84.
[15] T. Higaki, C. Liu, C. Zeng, R. Jin, Y. Chen, N. L. Rosi, R. Jin, *Angew. Chem. Int. Ed.* **2016**, *55*, 6694–6697; *Angew. Chem.* **2016**, *128*, 6806.
[16] R. Jin, *Nanoscale* **2010**, *2*, 343–362.
[17] R. Weissleder, *Nat. Biotechnol.* **2001**, *19*, 316–317.

[18] M. Zhu, E. Lanni, N. Garg, M. E. Bier, R. Jin, *J. Am. Chem. Soc.* **2008**, *130*, 1138–1139.
[19] M. Brust, M. Walker, D. Bethell, D. J. Schiffrin, R. Whyman, *J. Chem. Soc., Chem. Commun.* **1994**, 801–802.
[20] a) T. G. Schaaff, M. N. Shafigullin, J. T. Khoury, I. Vezmar, R. L. Whetten, W. G. Cullen, P. N. First, C. Gutiérrez-Wing, J. Ascensio, M. J. Jose-Yacamán, *J. Phys. Chem. B* **1997**, *101*, 7885–7891; b) T. G. Schaaff, G. Knight, M. N. Shafigullin, R. F. Borkman, R. L. Whetten, *J. Phys. Chem. B* **1998**, *102*, 10643–10646; c) M. W. Heaven, A. Dass, P. S. White, K. M. Holt, R. W. Murray, *J. Am. Chem. Soc.* **2008**, *130*, 3754–3755.
[21] Y. Negishi, K. Nobusada, T. Tsukuda, *J. Am. Chem. Soc.* **2005**, *127*, 5261–5270.
[22] Z. Wu, J. Suhan, R. Jin, *J. Mater. Chem.* **2009**, *19*, 622–626.
[23] R. Jin, H. Qian, Z. Wu, Y. Zhu, M. Zhu, A. Mohanty, N. Garg, *J. Phys. Chem. Lett.* **2010**, *1*, 2903–2910.
[24] a) Y. Yu, Z. Luo, Y. Yu, J. Y. Lee, J. Xie, *ACS Nano* **2012**, *6*, 7920–7927; b) T. Chen, J. Xie, *Chem. Rec.* **2016**, *16*, 1761–1771.
[25] X. Yuan, B. Zhang, Z. Luo, Q. Yao, D. T. Leong, N. Yan, J. Xie, *Angew. Chem. Int. Ed.* **2014**, *53*, 4623–4627; *Angew. Chem.* **2014**, *126*, 4711.
[26] a) M. Montalti, L. Prodi, N. Zaccheroni, G. Battistini, *Langmuir* **2004**, *20*, 7884–7886; b) M. Montalti, L. Prodi, N. Zaccheroni, R. Baxter, G. Teobaldi, F. Zerbetto, *Langmuir* **2003**, *19*, 5172–5174.
[27] C. Zeng, Y. Chen, A. Das, R. Jin, *J. Phys. Chem. Lett.* **2015**, *6*, 2976–2986.
[28] a) J. Jung, S. Kang, Y.-K. Han, *Nanoscale* **2012**, *4*, 4206–4210; b) Y. Li, G. Galli, F. Gygi, *ACS Nano* **2008**, *2*, 1896–1902.
[29] H. Qian, W. T. Eckenhoff, Y. Zhu, T. Pintauer, R. Jin, *J. Am. Chem. Soc.* **2010**, *132*, 8280–8281.
[30] A. Das, T. Li, K. Nobusada, C. Zeng, N. L. Rosi, R. Jin, *J. Am. Chem. Soc.* **2013**, *135*, 18264–18267.
[31] P. D. Jadzinsky, G. Calero, C. J. Ackerson, D. A. Bushnell, R. D. Kornberg, *Science* **2007**, *318*, 430–433.
[32] K. Salorinne, S. Malola, O. A. Wong, C. D. Rithner, X. Chen, C. J. Ackerson, H. Häkkinen, *Nat. Commun.* **2016**, *7*, 10401.
[33] M. Zhu, C. M. Aikens, F. J. Hollander, G. C. Schatz, R. Jin, *J. Am. Chem. Soc.* **2008**, *130*, 5883–5885.
[34] A. Vincenzo, P. Roberto, F. Marco, M. M. Onofrio, I. Maria Antonia, *J. Phys. Condens. Matter* **2017**, *29*, 203002.
[35] a) Z. Wu, J. Chen, R. Jin, *Adv. Funct. Mater.* **2011**, *21*, 177–183; b) J. B. Tracy, G. Kalyuzhny, M. C. Crowe, R. Balasubramanian, J.-P. Choi, R. W. Murray, *J. Am. Chem. Soc.* **2007**, *129*, 6706–6707.
[36] D.-e. Jiang, M. Kühn, Q. Tang, F. Weigend, *J. Phys. Chem. Lett.* **2014**, *5*, 3286–3289.
[37] C. M. Aikens, *J. Phys. Chem. Lett.* **2010**, *1*, 2594–2599.
[38] S. Knoppe, S. Malola, L. Lehtovaara, T. Bürgi, H. Häkkinen, *J. Phys. Chem. A* **2013**, *117*, 10526–10533.
[39] C. Zeng, C. Liu, Y. Pei, R. Jin, *ACS Nano* **2013**, *7*, 6138–6145.
[40] a) Y. Pei, Y. Gao, X. C. Zeng, *J. Am. Chem. Soc.* **2008**, *130*, 7830–7832; b) O. Lopez-Acevedo, H. Tsunoyama, T. Tsukuda, H. Häkkinen, C. M. Aikens, *J. Am. Chem. Soc.* **2010**, *132*, 8210–8218.
[41] K. L. D. M. Weerawardene, C. M. Aikens, *J. Phys. Chem. C* **2016**, *120*, 8354–8363.
[42] A. Kim, C. Zeng, M. Zhou, R. Jin, *Particle Particle Systems Characterization* **2017**, *34*, 1600388.
[43] S. Chen, S. Wang, J. Zhong, Y. Song, J. Zhang, H. Sheng, Y. Pei, M. Zhu, *Angew. Chem. Int. Ed.* **2015**, *54*, 3145–3149; *Angew. Chem.* **2015**, *127*, 3188.
[44] a) L. M. Tvedte, C. J. Ackerson, *J. Phys. Chem. A* **2014**, *118*, 8124–8128; b) C. J. Ackerson, R. D. Powell, J. F. Hainfeld, *Methods Enzymol.* **2010**, *481*, 195–230.
[45] S. Wang, X. Zhu, T. Cao, M. Zhu, *Nanoscale* **2014**, *6*, 5777–5781.
[46] a) H. C. Weissker, H. B. Escobar, V. D. Thanthirige, K. Kwak, D. Lee, G. Ramakrishna, R. L. Whetten, X. López-Lozano, *Nat. Commun.* **2014**, *5*, 3785; b) O. Lopez-Acevedo, J. Akola, R. L. Whetten, H. Gronbeck, H. Hakkinen, *Abstr. Pap. Am. Chem. Soc.* **2009**, *238*, 1; c) H. Qian, R. Jin, *Nano Lett.* **2009**, *9*, 4083–4087.
[47] J. Zheng, C. Zhou, M. Yu, J. Liu, *Nanoscale* **2012**, *4*, 4073–4083.
[48] a) J. Zheng, C. Zhang, R. M. Dickson, *Phys. Rev. Lett.* **2004**, *93*, 077402; b) J. Zheng, P. R. Nicovich, R. M. Dickson, *Annu. Rev. Phys. Chem.* **2007**, *58*, 409–431.
[49] R. D. Senanayake, A. V. Akimov, C. M. Aikens, *J. Phys. Chem. C* **2017**, *121*, 10653–10662.
[50] R. Johnston, P. Pyykko, *Chem. Soc. Rev.* **2008**, *37*, 1967–1997.
[51] W. A. de Heer, *Rev. Mod. Phys.* **1993**, *65*, 611–676.
[52] G. Wang, T. Huang, R. W. Murray, L. Menard, R. G. Nuzzo, *J. Am. Chem. Soc.* **2005**, *127*, 812–813.
[53] S. E. Crawford, C. M. Andolina, A. M. Smith, L. E. Marbella, K. A. Johnston, P. J. Straney, M. J. Hartmann, J. E. Millstone, *J. Am. Chem. Soc.* **2015**, *137*, 14423–14429.
[54] G. Wang, R. Guo, G. Kalyuzhny, J.-P. Choi, R. W. Murray, *J. Phys. Chem. B* **2006**, *110*, 20282–20289.
[55] L. Li, Z. Li, H. Zhang, S. Zhang, I. Majeed, B. Tan, *Nanoscale* **2013**, *5*, 1986–1992.
[56] S. Palmal, S. K. Basiruddin, A. R. Maity, S. C. Ray, N. R. Jana, *Chem. Eur. J.* **2013**, *19*, 943–949.
[57] X. Wen, P. Yu, Y.-R. Toh, A.-C. Hsu, Y.-C. Lee, J. Tang, *J. Phys. Chem. C* **2012**, *116*, 19032–19038.
[58] Z. K. Wu, M. Wang, J. Yang, X. H. Zheng, W. P. Cai, G. W. Meng, H. F. Qian, H. M. Wang, R. C. Jin, *Small* **2012**, *8*, 2028–2035.
[59] J. M. Forward, D. Bohmann, J. P. Fackler, R. J. Staples, *Inorg. Chem.* **1995**, *34*, 6330–6336.
[60] a) Z. Luo, X. Yuan, Y. Yu, Q. Zhang, D. T. Leong, J. Y. Lee, J. Xie, *J. Am. Chem. Soc.* **2012**, *134*, 16662–16670; b) N. Goswami, F. X. Lin, Y. B. Liu, D. T. Leong, J. P. Xie, *Chem. Mater.* **2016**, *28*, 4009–4016.
[61] S.-H. Cha, J.-U. Kim, K.-H. Kim, J.-C. Lee, *Chem. Mater.* **2007**, *19*, 6297–6303.
[62] M. S. Devadas, J. Kim, E. Sinn, D. Lee, T. Goodson, G. Ramakrishna, *J. Phys. Chem. C* **2010**, *114*, 22417–22423.
[63] a) S. H. Yau, O. Varnavski, J. D. Gilbertson, B. Chandler, G. Ramakrishna, T. Goodson, *J. Phys. Chem. C* **2010**, *114*, 15979–15985; b) S. H. Yau, O. Varnavski, T. Goodson, *Acc. Chem. Res.* **2013**, *46*, 1506–1516.
[64] C. Zhou, C. Sun, M. Yu, Y. Qin, J. Wang, M. Kim, J. Zheng, *J. Phys. Chem. C* **2010**, *114*, 7727–7732.
[65] X. Wen, P. Yu, Y.-R. Toh, J. Tang, *J. Phys. Chem. C* **2012**, *116*, 11830–11836.
[66] a) T. P. Bigioni, R. L. Whetten, Ö. Dag, *J. Phys. Chem. B* **2000**, *104*, 6983–6986; b) S. Link, A. Beeby, S. FitzGerald, M. A. El-Sayed, T. G. Schaaff, R. L. Whetten, *J. Phys. Chem. B* **2002**, *106*, 3410–3415.
[67] W. I. Lee, Y. Bae, A. J. Bard, *J. Am. Chem. Soc.* **2004**, *126*, 8358–8359.
[68] K. Pyo, V. D. Thanthirige, K. Kwak, P. Pandurangan, G. Ramakrishna, D. Lee, *J. Am. Chem. Soc.* **2015**, *137*, 8244–8250.
[69] Z. Tang, T. Ahuja, S. Wang, G. Wang, *Nanoscale* **2012**, *4*, 4119–4124.
[70] F. Aldeek, M. A. H. Muhammed, G. Palui, N. Zhan, H. Mattoussi, *ACS Nano* **2013**, *7*, 2509–2521.
[71] S. Zhou, Y. Duan, F. Wang, C. Wang, *Nanoscale* **2017**, *9*, 4981–4988.
[72] J. Jiang, C. V. Conroy, M. M. Kvetny, G. J. Lake, J. W. Padelford, T. Ahuja, G. Wang, *J. Phys. Chem. C* **2014**, *118*, 20680–20687.
[73] C. V. Conroy, J. Jiang, C. Zhang, T. Ahuja, Z. Tang, C. A. Prickett, J. J. Yang, G. Wang, *Nanoscale* **2014**, *6*, 7416–7423.
[74] Y. Yu, Z. Luo, D. M. Chevrier, D. T. Leong, P. Zhang, D.-e. Jiang, J. Xie, *J. Am. Chem. Soc.* **2014**, *136*, 1246–1249.
[75] K. Pyo, V. D. Thanthirige, S. Y. Yoon, G. Ramakrishna, D. Lee, *Nanoscale* **2016**, *8*, 20008–20016.
[76] S. Palmal, N. R. Jana, *Wiley Interdiscip. Rev. Nanomed. Nanobiotechnol.* **2014**, *6*, 102–110.
[77] X. D. Zhang, J. Chen, Z. T. Luo, D. Wu, X. Shen, S. S. Song, Y. M. Sun, P. X. Liu, J. Zhao, S. D. Huo, S. J. Fan, F. Y. Fan, X. J. Liang, J. P. Xie, *Adv. Healthcare Mater.* **2014**, *3*, 133–141.
[78] J. Xie, Y. Zheng, J. Y. Ying, *J. Am. Chem. Soc.* **2009**, *131*, 888–889.
[79] G. Guan, S.-Y. Zhang, Y. Cai, S. Liu, M. S. Bharathi, M. Low, Y. Yu, J. Xie, Y. Zheng, Y.-W. Zhang, M.-Y. Han, *Chem. Commun.* **2014**, *50*, 5703–5705.
[80] L. Gong, Z. L. Zhao, Y. F. Lv, S. Y. Huan, T. Fu, X. B. Zhang, G. L. Shen, R. Q. Yu, *Chem. Commun.* **2015**, *51*, 979–995.
[81] X. Le Guével, B. Hötzer, G. Jung, K. Hollemeyer, V. Trouillet, M. Schneider, *J. Phys. Chem. C* **2011**, *115*, 10955–10963.
[82] H. Kawasaki, K. Hamaguchi, I. Osaka, R. Arakawa, *Adv. Funct. Mater.* **2011**, *21*, 3508–3515.
[83] S. Volden, S. M. Lystvet, O. Halskau, W. R. Glomm, *RSC Adv.* **2012**, *2*, 11704–11711.

[84] C.-L. Liu, H.-T. Wu, Y.-H. Hsiao, C.-W. Lai, C.-W. Shih, Y.-K. Peng, K.-C. Tang, H.-W. Chang, Y.-C. Chien, J.-K. Hsiao, J.-T. Cheng, P.-T. Chou, *Angew. Chem. Int. Ed.* **2011**, *50*, 7056–7060; *Angew. Chem.* **2011**, *123*, 7194.

[85] a) H. Wei, Z. Wang, L. Yang, S. Tian, C. Hou, Y. Lu, *Analyst* **2010**, *135*, 1406–1410; b) W.-Y. Chen, J.-Y. Lin, W.-J. Chen, L. Luo, E. Wei-Guang Diau, Y.-C. Chen, *Nanomedicine* **2010**, *5*, 755–764; c) T.-H. Chen, W.-L. Tseng, *Small* **2012**, *8*, 1912–1919; d) B. A. Russell, B. Jachimska, P. Komorek, P. A. Mulheran, Y. Chen, *Phys. Chem. Chem. Phys.* **2017**, *19*, 7228–7235.

[86] C. Sun, H. Yang, Y. Yuan, X. Tian, L. Wang, Y. Guo, L. Xu, J. Lei, N. Gao, G. J. Anderson, X.-J. Liang, C. Chen, Y. Zhao, G. Nie, *J. Am. Chem. Soc.* **2011**, *133*, 8617–8624.

[87] Y. Wang, J.-T. Chen, X.-P. Yan, *Anal. Chem.* **2013**, *85*, 2529–2535.

[88] P. L. Xavier, K. Chaudhari, P. K. Verma, S. K. Pal, T. Pradeep, *Nanoscale* **2010**, *2*, 2769–2776.

[89] A. L. West, M. H. Griep, D. P. Cole, S. P. Karna, *Anal. Chem.* **2014**, *86*, 7377–7382.

[90] Y. Kong, J. Chen, F. Gao, R. Brydson, B. Johnson, G. Heath, Y. Zhang, L. Wu, D. Zhou, *Nanoscale* **2013**, *5*, 1009–1017.

[91] a) H. Wei, Z. Wang, J. Zhang, S. House, Y.-G. Gao, L. Yang, H. Robinson, L. H. Tan, H. Xing, C. Hou, I. M. Robertson, J.-M. Zuo, Y. Lu, *Nat. Nanotechnol.* **2011**, *6*, 93–97; b) K. Chaudhari, P. L. Xavier, T. Pradeep, *ACS Nano* **2011**, *5*, 8816–8827.

[92] A. Yahia-Ammar, D. Sierra, F. Merola, N. Hildebrandt, X. Le Guevel, *ACS Nano* **2016**, *10*, 2591–2599.

[93] Y. Negishi, T. Iwai, M. Ide, *Chem. Commun.* **2010**, *46*, 4713–4715.

[94] S. Wang, X. Meng, A. Das, T. Li, Y. Song, T. Cao, X. Zhu, M. Zhu, R. Jin, *Angew. Chem. Int. Ed.* **2014**, *53*, 2376–2380; *Angew. Chem.* **2014**, *126*, 2408.

[95] G. Soldan, M. A. Aljuhani, M. S. Bootharaju, L. G. AbdulHalim, M. R. Parida, A. H. Emwas, O. F. Mohammed, O. M. Bakr, *Angew. Chem. Int. Ed.* **2016**, *55*, 5749–5753; *Angew. Chem.* **2016**, *128*, 5843.

[96] Y. M. Guo, F. P. Cao, X. L. Lei, L. H. Mang, S. J. Cheng, J. T. Song, *Nanoscale* **2016**, *8*, 4852–4863.

[97] X. Kang, S. X. Wang, Y. B. Song, S. Jin, G. D. Sun, H. Z. Yu, M. Z. Zhu, *Angew. Chem. Int. Ed.* **2016**, *55*, 3611–3614; *Angew. Chem.* **2016**, *128*, 3675.

[98] M. Montalti, N. Zaccheroni, L. Prodi, N. O'Reilly, S. L. James, *J. Am. Chem. Soc.* **2007**, *129*, 2418–2419.

[99] S. Bonacchi, A. Cantelli, G. Battistelli, G. Guidetti, M. Calvaresi, J. Manzi, L. Gabrielli, F. Ramadori, A. Gambarin, F. Mancin, M. Montalti, *Angew. Chem. Int. Ed.* **2016**, *55*, 11064–11068; *Angew. Chem.* **2016**, *128*, 11230.

[100] W. W. Weare, S. M. Reed, M. G. Warner, J. E. Hutchison, *J. Am. Chem. Soc.* **2000**, *122*, 12890–12891.

[101] a) M. Montalti, L. S. Dolci, L. Prodi, N. Zaccheroni, M. C. A. Stuart, K. J. C. van Bommel, A. Friggeri, *Langmuir* **2006**, *22*, 2299–2303; b) S. Bonacchi, E. Rampazzo, M. Montalti, L. Prodi, N. Zaccheroni, F. Mancin, P. Teolato, *Langmuir* **2008**, *24*, 8387–8392.

Received: June 21, 2017